ACS NANOSCIENCE Au
AN OPEN ACCESS JOURNAL OF THE AMERICAN CHEMICAL SOCIETY

pubs.acs.org/nanoau
Article

Biphosphor Carbon Dots/Chlorophyll System Entirely Derived from *Chlorella* Microalgae for Luminescent Solar Concentrators

Published as part of ACS Nanoscience Au special issue "Advances in Energy Conversion and Storage at the Nanoscale."

Filipe M. Santos,* Tiago A. G. Duarte,¶ Sandra F. H. Correia,¶ Rui F. P. Pereira,¶ Alexandra Conde, Álvaro R. Ribeiro, Susana Santos Braga, Sónia P. M. Ventura, Rute A. S. Ferreira, Verónica de Zea Bermudez, and Sílvia C. Nunes

Cite This: https://doi.org/10.1021/acsnanoscienceau.4c00048

Read Online

ACCESS | Metrics & More | Article Recommendations | Supporting Information

ABSTRACT: In this work, a singular system capable of interacting with the entire visible region of the solar spectrum is produced by combining carbon dots (CDs) and chlorophyll (Chl) pigments, entirely derived from the microalga *Chlorella pyrenoidosa*. The process involves the digestion of the *C. pyrenoidosa* cellular wall in an acetic acid:cholinium chloride (AA/ChCl) solvent, followed by a microwave reaction. The resulting CDs exhibit excitation and emission maxima at 461 and 528 nm, respectively. The Chl centers enable a secondary photoluminescence (PL) process, thus ensuring that the as-prepared CDs/Chl system (CDCS) can also interact with the farther red region of the visible spectrum. The luminescence properties of CDCS are concentration-dependent, undergoing a blue shift with dilution. Confocal microscopy provided insights into the protection of Chl pigments throughout the process. Furthermore, the consequences arising from the addition of poly(ethylene glycol) oligomers (PEG-200) are also analyzed. The results demonstrate that the interaction between CDCS and PEG-200 significantly modifies the PL intensity and emission wavelengths, especially at higher PEG-200 concentrations. This suggests that PEG-200 can act as a modulating agent, stabilizing and even preventing the CDs' fluorescence quenching while also affecting the PL properties of Chl. This work presents interesting possibilities for the development of multifunctional luminescent systems derived from microalgae biomass by addressing how these microorganisms can function not only as precursors in the formation of advanced functional materials but also as an integrated component of these systems. As an added benefit, a luminescent solar concentrator (LSC) was fabricated, revealing photostability, as well as optical and power conversion efficiency values of 11 and 0.2%, respectively, values comparable to state-of-the-art CD-based LSCs.

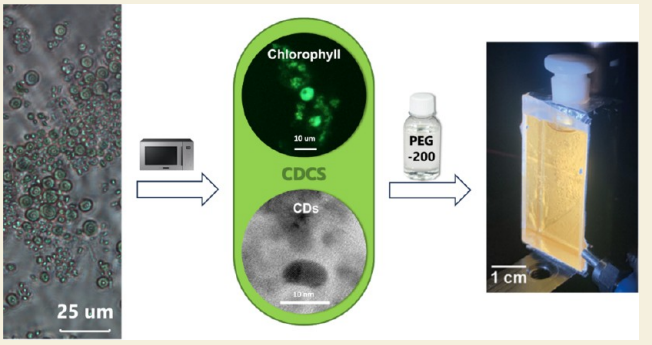

KEYWORDS: *Chlorella pyrenoidosa, microalgae, carbon dots, chlorophyll, PEG, luminescent solar concentrators*

1. INTRODUCTION

One of the most attractive ideas about using unicellular organisms as carbon dot (CD) precursors is that everything needed to obtain our nanomaterials is contained inside one small capsule. All that is required is to break that capsule, allow its contents to pour into the reaction vessel, and proceed with CD synthesis.

This idea was put into practice in the present work in the framework of a project devoted to the active layers of luminescent solar concentrators (LSCs) for building-integrated photovoltaic (BIPV) technology.[1,2] BIPVs represent an appealing strategy to address the 2050 European targets for energy performance and ensure the transition to net-zero emissions.[3] These concerns are intimately associated with the urban environment, since buildings are major energy consumers. LSCs belong to a group of devices, usually known as spectral converters, that are meant to improve the applicability of photovoltaic (PV) cells.[4]

An archetypal LSC comprises a planar waveguide coated and doped with highly emissive chromophores. Sunlight is absorbed by the chromophore species and re-emitted at a longer wavelength. The emitted light then propagates to the

Received: July 31, 2024
Revised: November 27, 2024
Accepted: December 2, 2024

Scheme 1. Preparation Process of the CDCS (2), from the Microalga *C. pyrenoidosa* (1)[a]

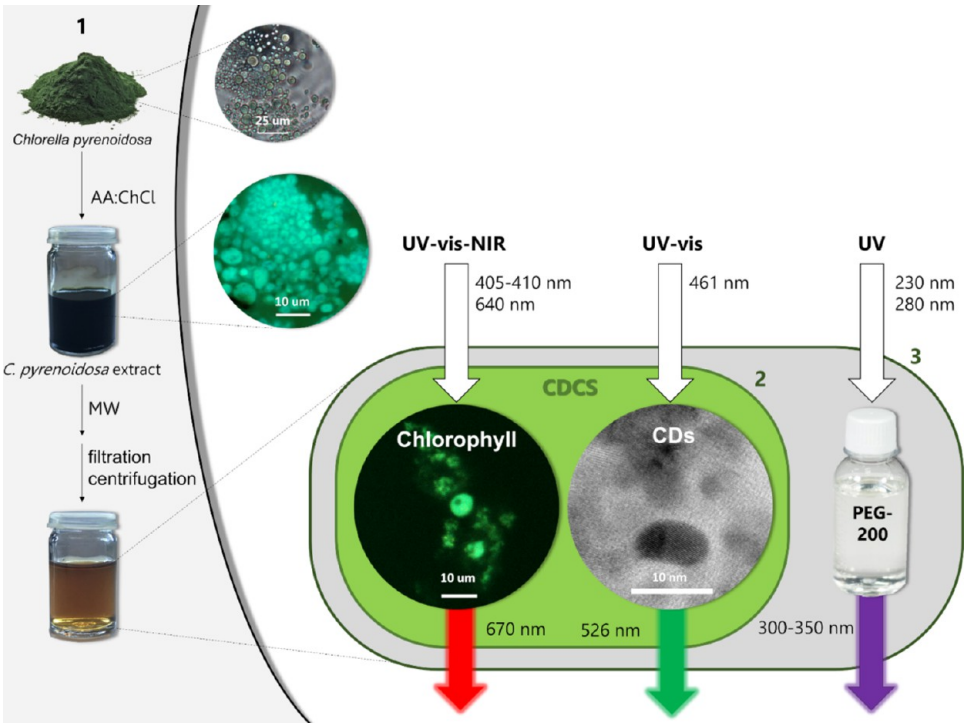

[a]After digestion, with an AA/ChCl (16:1) solvent, the solution underwent a microwave (MW) reaction to produce the CDCS. The latter system was eventually combined with PEG-200 to yield (**3**).

waveguide edges by total internal reflection, where small PV cells convert it into electricity.[4] The efficiency of the LSCs depends critically on the optical processes in the devices. The losses associated with the optically active center include nonabsorbed photons, emission quantum yield (Φ) < 100%, and reabsorption of emitted photons by neighboring optically active centers, mainly owing to small Stokes shift values. LSCs offer a series of benefits, an important one being the design of devices with both tunable transmittance and uniform transparency. In addition, they are particularly suitable for integration in metropolitan areas since they can harvest direct and diffuse radiation, and their operation is not jeopardized under shading conditions. The design of LSCs needs to fulfill a series of requirements. Such materials should possess a high molar extinction coefficient (ε), high emission quantum yield (Φ > 50%), high brightness ($B = \Phi \times \varepsilon$), and large Stokes shift. Furthermore, the emitted photon energy should match the spectral absorption of the silicon (Si) PV cell. Ideally, LSCs should absorb in the UV-blue region and emit in the red/near-infrared (NIR) region.[5,6]

CDs are among the most interesting emitting centers for LSCs.[7−10] CDs ally their excellent photoluminescence (PL) features, photostability, high aqueous dispersibility, good thermal stability, and chemical inertness with the nowadays increasingly relevant qualities of low toxicity, favorable biocompatibility, and environment-friendly nature, all of which are anchored in facile synthetic procedures and great flexibility of surface modification.[11−14] CDs are zero-dimensional (0D), quasi-spherical nanoparticles with a carbon-based core exhibiting various functional groups at the surface level.[11,12] They can be prepared by several methods from all kinds of organic precursors, ranging from simple natural products (e.g., citric acid, urea, glucose) to complex materials like waste, plant biomass, and food items.[14,15] In either case, these affordable raw materials provide not only the necessary carbon sources but can also afford a supply of different heteroatoms—such as sulfur (S), nitrogen (N), and phosphorus (P)—enhancing CD functionality and addressing environmental concerns related with their disposal and treatment.[14,16]

Organic colorants are also important emitters for LSCs,[7,17] as they can cover a significant part of the solar spectrum and offer high absorption coefficients, broad emission bands, and strong quantum yields. They are made of carbon-based molecules; while most colorants are soluble (dyes), some are not (pigments). However, they are not environmentally friendly, have small Stokes shifts, and suffer from significant reabsorption.[17] Interestingly, some biosourced colorants (e.g., chlorophyll (Chl), phycobiliproteins) have been successfully used in LSC devices.[18−20] This concept of biosourcing colorants aligns with the increasing emphasis on sustainability and green synthesis, encouraging the use of abundant natural raw materials. From here, it follows that by carefully selecting both the biomass precursors and the experimental conditions used for the CDs' production, the added benefit of the presence of these natural colorants could also be a possibility.

Microalgae are emerging as innovative tools,[21−23] finding applications in fields beyond health and wellness,[24,25] such as bioplastics,[26,27] pollution control and waste management,[28,29] and sustainable energy.[30,31] Empowering all of this research are unicellular, photosynthetic microorganisms with a remarkable ability to rapidly grow and flourish in various aquatic environments due to their simple structure. Containing high amounts of valuable phytochemicals of interest (e.g., polysaccharides, proteins, lipids, pigments), microalgae are a rich source of bioactive materials.[32,33]

https://doi.org/10.1021/acsnanoscienceau.4c00048
ACS Nanosci. Au XXXX, XXX, XXX−XXX

Although the green microalgae *Chlorella pyrenoidosa* stands out for its commercial exploitation as a food supplement,[34,35] there is also growing interest in its use as a CD precursor.[36−39] However, its valuable components are trapped inside robust cell walls, requiring pretreatment for extraction.[40,41] Several studies have explored using water or ethanol as solvents for CD synthesis from microalgae.[42−45] For alternative solvents, such as eutectic solvents (ESs), research is still scarce,[46−48] notwithstanding their versatility in the pretreatment and/or conversion of biomass into value-added products.[49,50] ESs result from the self-association of two or more compounds at specific molar ratios, predominantly through hydrogen bonding between a hydrogen bond donor and a hydrogen bond acceptor. This interaction results in a system with a lower melting point than its pure components.[51−53] ESs can easily be prepared from a vast library of compounds—which includes ubiquitous naturally occurring compounds (e.g., cholinium (Ch^+) sugars, natural carboxylic acids, polyols)[54,55]—allowing the design of systems with specific, tunable properties.[51−53]

In the present work, a two-component chromophore platform was derived from *C. pyreonoidosa* microalgae. CDs were obtained using an acetic acid: cholinium chloride (AA/ChCl) ES (Figure S1 in Supporting Information) as an all-purpose medium for the whole process regarding the conversion of *C. pyrenoidosa* biomass to CDs ((**1**) in Scheme 1). The second component, Chl, was a logical choice due to its inherent presence in the microalgae *C. pyrenoidosa*. This pigment is deeply involved in plants' sunlight harvesting and the conversion of the absorbed photons into chemical energy, thus playing a pivotal role in photosynthesis. Chls are porphyrin derivatives with a central magnesium cation chelated into the aromatic structure. They have a characteristic red/NIR emission at 660−680 and 720 nm, associated with their monomer chlorophyll a (Chl-a) and dimeric contributions, respectively.[56,57]

Additionally, a third component was introduced in the form of aqueous poly(ethylene glycol) (PEG) solutions. With known applications in various fields of science (e.g., biotechnology and biomedical science, materials science, organic synthesis), PEGs are a very attractive class of synthetic polymers.[58,59] They have a set of benign characteristics (e.g., low toxicity, high biocompatibility, high water solubility) approved by the Food and Drug Administration for various biomedical uses, including internal consumption.[59] It is noteworthy that they have been consistently explored as precursors, solvents/matrices, or passivating agents in the synthesis of CDs and other nanoparticles.[59] More recently, they were found to exhibit rather strong luminescence,[60,61] despite being organic molecules devoid of conjugated π systems or fluorophores. However, their use as a CDs' dispersion medium was only briefly explored, even though they succeeded in enhancing the CDs' PL properties, such as peak wavelength, PL intensity, and electron time decay.[62]

The resulting CDs/Chl system (CDCS) water and PEG solutions were used to fabricate a planar LSC with state-of-the-art performance.

2. EXPERIMENTAL SECTION

2.1. Reagents

Dried *C. pyrenoidosa* was obtained from a commercial source. Glacial AA (extra pure, 99.7+%, SLR, meets analytical specification of Ph.Eur., BP, USP) and ChCl (98+%; 3% water, as measured by thermogravimetric analysis (TGA)) were purchased from Fisher Chemical. Sodium hydroxide (NaOH, Eka Chemicals pellets), PEG (average molecular weight (M_W): 200 g mol^{-1}, for synthesis, Sigma-Aldrich), and all remaining reagents were of analytical grade or higher and were used as received. Distilled water was used throughout.

2.2. Synthetic Procedures

2.2.1. Solvent Preparation. The synthetic procedure proposed by Pan et al.[63] was followed. The AA/ChCl solvent was prepared by mixing glacial AA (100 mL; 1.74 mol) and ChCl (15.65 g, corresponding to 15.05 g or 0.108 mol of pure ChCl) inside a 100 mL flask, which corresponds to an AA/ChCl molar ratio of 16:1. The mixture was then heated at 50 °C with continuous stirring until full homogenization was observed.

2.2.2. Preparation of CDs from the Algal Precursor. 1.5 g of dried *C. pyrenoidosa* was immersed in 15 mL of the AA/ChCl (16:1) solvent and left for 24 h at room temperature under stirring inside a sealed, light-protected flask. The resulting mixture was then placed in a SAMSUNG domestic MW apparatus and allowed to react for 2 min at 450 W power. Afterward, 10 mL of water was added to the resulting semidried slurry, and NaOH 1 M solution was used to neutralize the excess acidity. This mixture was then filtered and twice-centrifuged (4000 rpm, 20 min) to obtain CDCS.

2.2.3. Preparation of CDs from the Solvent (Experimental Control). A 15 mL portion of the AA/ChCl (16:1) solvent was directly placed inside the SAMSUNG domestic MW and allowed to react for 5 min at 450 W. This step was followed by addition of 10 mL of water to the dried residue, neutralization with NaOH (1 M), filtration, and centrifugation at 4000 rpm for 20 min. In the end, a clear solution containing the CDs (designated as CDS hereafter) was obtained.

2.2.4. Preparation of CDs from a Chl Ethanolic Extract (Experimental Control). A 2 mL portion of a Chl ethanolic extract was added with 15 mL of the AA/ChCl (16:1) solvent for 24 h at room temperature. The CD formation for the algal precursor was then carried out exactly as reported above.

2.2.5. Effect of PEG-200 in the CDCS. For the optical studies, several aliquots of PEG-200 were weighed and directly added to 5 g of the CDCS aqueous solution (see Table S3). The resulting solution was then gently stirred until full homogenization. To obtain the 100% PEG-200 CDCS solution, 5 g of the prepared aqueous solution was lyophilized. Then, 5.5 g of PEG-200 was added to the resulting powder with stirring until full dissolution.

2.3. Structural and Optical Characterization

Attenuated total reflectance Fourier transform infrared (ATR-FTIR) spectra were recorded with an IRaffinity-1S Shimadzu spectrometer equipped with a horizontal unique reflection ATR accessory (Golden Gate). The spectra were recorded with 128 scans between 4000 and 400 cm^{-1} with a resolution of 4 cm^{-1}. Additional FTIR spectra were collected by using a Thermo Scientific Nicolet iS10 spectrometer with a smart iTR accessory, covering the 4000−600 cm^{-1} range. The spectra were obtained by averaging 128 scans at a resolution of 4 cm^{-1}. Approximately 2 mg of the sample was finely ground, mixed with ∼175 mg of predried potassium bromide (KBr, Merck, spectroscopic grade) in an agate mortar, and then pressed into pellets.

TGA was carried out in a DTA/TGA Netsch STA 449F3 thermal analyzer. In a typical experiment, samples were heated from room temperature to 700 °C in alumina (Al_2O_3) crucibles under a nitrogen (N_2) atmosphere (50 mL min^{-1} purge; 20 mL min^{-1} protective flow), at a heating rate of 10 °C min^{-1}.

Differential scanning calorimetry (DSC) experiments were performed in a PerkinElmer DSC7 calorimeter equipped with an intracooler cooling unit. The analyses were carried out using ca. 3 mg of the compound in 30 μL aluminum vented pans, in the temperature range from −140 to 20 °C, with a heating rate of 10 °C min^{-1} and a cooling rate of 20 °C min^{-1}. Dry N_2 at a 20 mL min^{-1} flow rate was used as the purge gas.

High-resolution transmission electron microscopy (HR-TEM) images were obtained at the INL—Iberian Nanotechnology Laboratory, using a JEOL JEM 2100 (200 kV). In a typical procedure, the samples were dispersed in a water vortex and then applied to a

https://doi.org/10.1021/acsnanoscienceau.4c00048
ACS Nanosci. Au XXXX, XXX, XXX−XXX

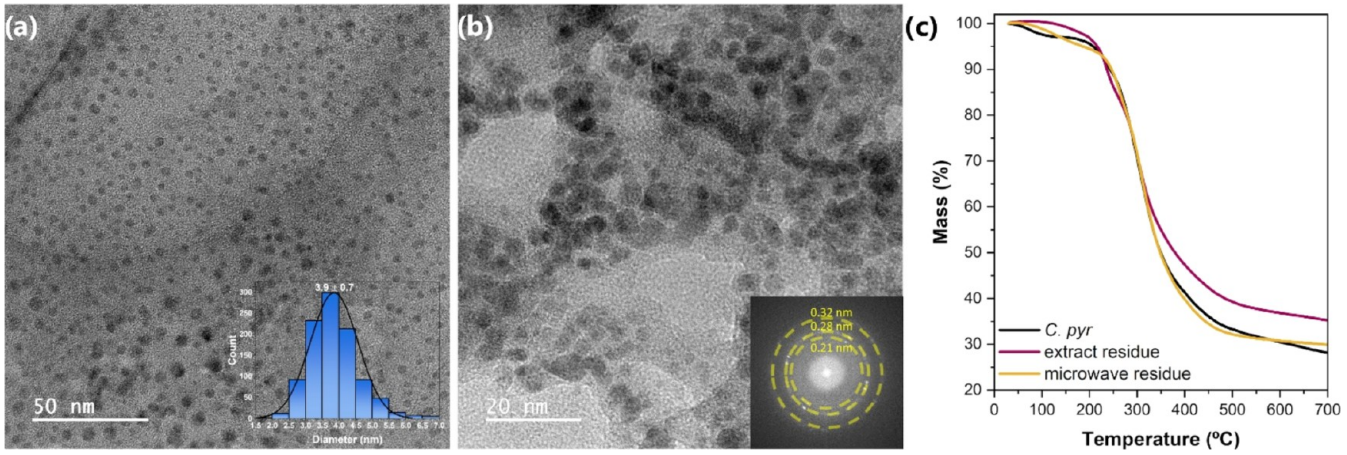

Figure 1. Characterization of the CDCS: (a, b) HR-TEM images. The inset of panel (a) shows the CDs' size distribution and that of panel (b) shows the SAED with the identified *d*-spacings (0.18, 0.21, 0.28, and 0.32 nm). The first two *d*-spacings correspond to the CDs, while the latter are due to the presence of sodium salts. (c) TGA curves of the *C. pyrenoidosa* microalga (black line), the extract residue (pink line), and the MW residue (yellow line).

400-mesh copper grid containing lacey carbon and an ultrathin carbon support film (Ted Pella ref 01824). Digital Micrograph software was used for Fast Fourier Transformation (FFT) analysis.

Confocal microscopy (CM) images were also obtained at INL—Iberian Nanotechnology Laboratory, with the help of a model LSM780 confocal laser scanning microscope from Carl Zeiss Microscopy, using a 63× plan-Apochromat oil-emerged objective, 1.4 NA (numerical aperture). In a typical experiment, 50 μL were pipetted into a chamber slide and placed under the microscope. Fluorescence excitation was achieved using several lasers, each operating on an independent channel, providing excitation wavelengths of 405, 488, and 633 nm. Images were acquired and processed with the Zeiss Zen software (Carl Zeiss Microscopy).

The powder X-ray diffraction analysis (PXRD) was conducted using a Rigaku DMAX III/C diffractometer by performing a 3−60° (2θ) scan in reflection mode, with an operating voltage of 30 kV and a current of 15 mA. Monochromated Cu K_α radiation (λ = 1.54 Å) was used. The solid was deposited onto a glass substrate.

Fluorescence spectra were recorded between 250 and 800 nm with a Varian Carey Eclipse Fluorescence spectrometer using a 10 mm quartz cuvette. The excitation and emission slit widths were all set at 5 nm. The obtained spectra were corrected for the system's wavelength response. The absolute emission quantum yield (Φ) values were measured at room temperature by using a C9920−02 Hamamatsu system. The method is accurate within 10%.

Ultraviolet−visible (UV−vis) absorption spectra were obtained between 220 and 900 nm with a Lamba 25 PerkinElmer spectrometer with the aid of a 1 cm quartz cuvette by using deionized water as a solvent.

2.4. Chl Quantification

The absorbance spectrum was analyzed using UV−vis spectrophotometry from 230 to 700 nm, by employing a UV−vis microplate reader (SpectraMax). Each sample was appropriately diluted in water, with a sample/water ratio of 1:100. The homogenization of the samples was achieved via vortex mixing, followed by the pipetting of 300 μL of each sample into individual microplate wells. Each sample was assayed in duplicate.

3. RESULTS AND DISCUSSION

3.1. CDCS

In this work, *C. pyrenoidosa* microalgae were used as precursors for the preparation of CDs. The choice was made for a commercial source instead of a specially developed strain, since it provided a low-cost option for the CD synthesis process by using a widely available source of biomass.

Generating *C. pyrenoidosa*-derived CDs entailed a two-step process consisting of a solid−liquid extraction procedure and a carbonization stage (Scheme 1). The extraction was performed with the AA/ChCl (16:1) solvent for 24 h, following a process similar to that described by Lu et al.[64] Although other authors have reported processes with shorter extraction times,[65−68] the main concern during the design of this experiment was not one of recovery of any extracted material but of availability of sufficient material to carbonize under mild conditions. Hence, by allowing the pretreatment to proceed for 24 h, we could ensure extraction and maximal digestion of all susceptible material. Moreover, the (AA/ChCl) system platform was chosen because of its previous use in the extraction of biocomponents from *C. pyrenoidosa*[65−69] and other species.[63,64,68] We note that the AA/ChCl (2:1) ES[63,66,70] was found to be too viscous for biomass extraction, which led to a dilution of up to 50% water.[70] Herein, we used a different proportion with a higher AA/ChCl molar ratio. This adjustment was done with a 2-fold objective: to lower the viscosity and thus eliminate the need for water while simultaneously facilitating the rupture of the microalgae cell wall—and the consequent extraction of higher amounts of biocomponents[63,67,71]—due to its more acidic nature.[63] In addition, strong acidic media are reported to afford a higher degree of surface oxidation in CDs with longer emission due to a smaller energy gap of surface states in the oxidized CDs.[72] To confirm the eutectic nature of the AA/ChCl (16:1) solvent herein employed, DSC and ATR-FTIR measurements were performed (Supporting Information).

The resulting dark-green solution (Figure S4a in the Supporting Information) was placed inside a MW oven. This process yielded a dark-green dried residue, which, after being dissolved in water and subjected to filtration and centrifugation, afforded a yellowish-brown solution (Figure S4b), characteristic of CDs, named CDCS hereafter ((**2**) in Scheme 1). All attempts to dialyze this solution invariably led to the loss of Chl content. Therefore, further purification through dialysis was avoided. Consequently, the present results concern the filtered aqueous solution obtained from MW treatment of the *C. pyrenoidosa* biomass.

By lyophilizing this solution, we obtained a light beige powder. The ATR-FTIR analysis of this powder (Table S1 and

https://doi.org/10.1021/acsnanoscienceau.4c00048
ACS Nanosci. Au XXXX, XXX, XXX−XXX

Figure S5, black, blue, red, and green lines, in the Supporting Information) confirmed the presence of the acetylcholinium cation in all samples, as indicated by the bands at 1741 and 1081 cm^{-1} (for a more complete discussion of the ATR-FTIR spectra, please refer to the Supporting Information). Additionally, a band located at 1569 cm^{-1} in the ATR-FTIR spectra of all of the CDCS samples (Figure S5, black, blue, red, and green lines) was attributed to the C=C stretching vibration, typical of sp^2 carbon structures, and indicative of the presence of CDs.[73]

As a control experiment, the AA/ChCl (16:1) solvent also underwent MW carbonization. However, the experimental conditions that afforded CDCS were insufficient to produce CDs from just the solvent alone (CDS). Hence, the reaction time was increased to 5 min while maintaining the same MW power, at which point CD formation, although minimal, could be observed. The ATR-FTIR spectrum of the lyophilized powder (Figure S5, violet line)—albeit different from those obtained for the CDCS samples—also indicated the presence of the acetylcholinium cation, and suggested a minimal presence of CDs (Supporting Information).

3.2. Morphology, Size, and Origin of the CDs

The HR-TEM images of the CDCS samples (Figures 1a,b and S6 in the Supporting Information) revealed a massive presence of sphere-shaped nanostructures with an average diameter of 3.9 ± 0.7 nm. Both the spherical shape and the size (less than 10 nm) provide unequivocal evidence of the presence of CDs. The produced CDs exhibit a crystalline structure with interplanar spacings of 0.18,[74,75] and 0.21[73] nm, which correspond to the (103) and (100) diffraction planes of graphitic carbon, respectively. Additionally, two other interplanar distances were found. The distance of 0.28 nm is attributed to the presence of sodium chloride (NaCl),[76] while that of 0.32 has been attributed to the (110) diffraction plane of sodium acetate (CH_3COONa).[77] Both sodium salts originate from the neutralization step with NaOH, and their presence was confirmed by PXRD (Figure S7 in the Supporting Information).

In contrast, the HR-TEM images of the CDS samples showed mostly undefined structures (Figure S8a,b in the Supporting Information), with only a trace presence of spherical nanostructures (Figure S8c). The detection of a small amount of CDs, even after a carbonization time of 5 min—which is more than double the time necessary for the CDCS to form—is clear evidence that the AA/ChCl (16:1) ES was not the main source of the CDs. Moreover, this confirms the ATR-FTIR results in which the band attributed to the presence of sp^2 carbon domains emerged as a shoulder.

To further confirm that the source of the CDs present in CDCS samples was derived from the phytochemicals in the microalgae extract, TGA experiments were performed on the microalgae extract and carbonization residues, and untreated biomass.

Typically, biomass pyrolysis under an N_2 atmosphere occurs in three main stages. The first event (between room temperature and *ca.* 150−200 °C) is associated with the loss of hydration waters. The second thermal event—where the mass loss rate is the highest—occurs between 200 and 500 °C. Finally, above 600 °C, the system evolves to the formation of carbon-containing species (CO_x, C_xH_y, and tars) until constant weight is reached.[78−80] While the degradation of carbohydrates and proteins under an inert atmosphere occurs during the second thermal stage, that of the lipids unfolds slowly at temperatures above 500 °C without the formation of a defined DTGA peak temperature. As to the decomposition of carbohydrates and proteins, although they take place at the same thermal event, each of them occurs independently, within a specific range of temperatures: nonfibrous carbohydrates decompose at temperatures between 190 and 270 °C, while protein degradation starts from ca. 270−370 °C.[80,81]

The TGA curves (Figure 1c) and their corresponding derivative (DTGA) curves for the microalgae material, before and after the extraction and MW stages (Figure S9 and Table S2, Supporting Information), reveal a degradation process occurring in three different steps, in excellent agreement with the thermal degradation process just described above. In brief, mass losses remained approximately at the same level for all three samples: 3−5% for Stage 1, 48−51% for Stage 2, and 13−19% for Stage 3 (Table S2). It is noteworthy that the amount of carbohydrate content that was degraded strongly increased from the *C. pyrenoidosa* biomass (7%) to the extract and MW residues (13 and 11%, respectively). Moreover, the DTGA peak located at 234 °C (Figure S9b) had its area significantly enlarged (Figure S9c), indicating a greater extent of carbohydrate degradation associated with the disruption of the cell wall of *C. pyrenoidosa*, as a result of the solvent's action during the extraction process. After the MW step—and the formation of CDs—the DTGA peak located at 234 °C (Figure S9b) shifted to 264 °C (Figure S9a,d), suggesting that a significant part of the leaked carbohydrates was consumed during the MW process. This leads us to conclude that the carbohydrates extracted from the *C. pyrenoidosa* microalgae are a significant source of the CDs described here, especially when taking into consideration the ATR-FTIR spectra of the lyophilized CDCS systems, which confirmed the presence of solvent-related entities.

Regarding the potential consumption of protein in the formation of the CDs, a comparison of the TGA/DTGA curves of the *C. pyrenoidosa* (Figure S9b) vis-à-vis the final residue (Figure S9d) reveals a striking similarity, suggesting that the protein content remained practically unchanged (Figure S9a). This strongly suggests that the contribution of proteins to the formation of CDs was minimal. This likeness is also evident in the TGA curves for the same samples (Figure 1c) and their identical residual masses (Table S2). This implies that the cellular structures present after the CDs' formation were essentially the same as those at the beginning of the process. From these observations, two conclusions can be drawn: first (arising from the close resemblance of the curves), all components susceptible to degradation and carbonization during the CD process were effectively transformed; second, there was likely more biomass available in the reaction mixture than what the solvent could reach and disrupt.

3.3. Optical Properties

The UV−vis absorption spectrum of the CDCS-4 sample displays two shoulders at 252 and 275 nm (Figure S10 in Supporting Information), attributed to the $\pi-\pi^*$ transitions associated with C=O and C=C groups.[73,82] These data correlate well with the reported ATR-FTIR data (Supporting Information). Moreover, a long, tailed absorption band extends from 300 nm to higher wavelengths, encompassing practically all of the vis region. This tail arises from several weak absorption bands originating from the various constituents of the CDCS. Noteworthy contributions include the Soret band

https://doi.org/10.1021/acsnanoscienceau.4c00048
ACS Nanosci. Au XXXX, XXX, XXX−XXX

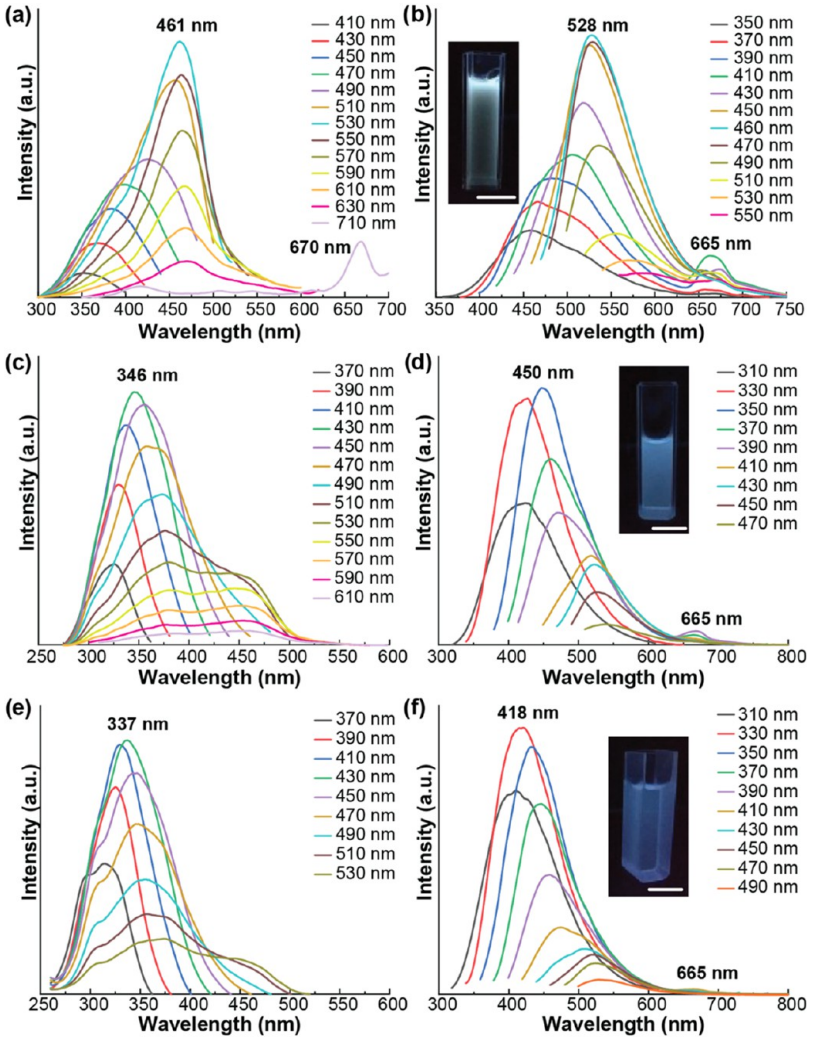

Figure 2. Optical properties of the CDCS-4 sample. PL spectra at various concentrations: (a) excitation and (b) emission spectra at maximum concentration; (c) excitation and (d) emission spectra for a 20% diluted solution; and (e) excitation and (f) emission spectra for the 8% diluted solution. The insets show pictures of the 10 mm quartz cuvette taken under a 365 nm lamp.

and the weaker absorption bands located between the Soret and the Q bands of Chl,[56,57,83] but also bands arising from the presence of different surface states in the CDs.[73,84,85]

Broad bands shift from 400 to 475 nm (Figure 2a) and from 490 to 610 nm (Figure 2b) in the excitation and emission spectra, respectively, at increasing excitation wavelengths, with the intensity maxima being attained at 461 and 528 nm in the excitation and emission spectra, respectively, with a Stokes shift of 67 nm. It is worth noting that these spectra show a huge improvement compared to the CDS spectra (Figure S11 in the Supporting Information). In the latter case, the excitation and emission maxima are markedly blue-shifted to 357 and 438 nm, respectively.

The UV−vis absorption spectra also reveal a band at 670 nm (Figure S11), indicating the presence of Chls. These can be easily distinguished by their two strong absorption bands: the Soret band, in the blue region between 400 and 460 nm, and the Q-band, in the red region, between 640 and 680 nm.[83,86] For *C. pyrenoidosa*, the main Chl component has been identified as Chl-a,[87,88] with bands centered around 420−440 and 660−670 nm.[83,86] Thus, the band at 670 nm is due to the presence of Chl-a. This colorant is also discerned in the PL spectra reproduced in Figure 2, with an excitation wavelength maximum at 640 nm—when it becomes the predominant fluorophore—for an emission at 667 nm.

Further investigation revealed that the PL properties of CDCS vary with the dilution of its solution. As shown in Figure 2, both the excitation and emission spectra can be significantly blue-shifted. When diluting the original solution to a fifth of its original concentration, i.e., 20% (Figure 2c,d), the excitation and emission spectra shift from 461 to 346 nm and 528 to 450 nm, respectively, with a Stokes shift of 104 nm. Further dilution to 8% leads to a further shift to 337 and 418 nm for the emission and excitation spectra, respectively, and a Stokes shift of 81 nm (Figure 2e,f). Concomitantly, the PL of the Chl chromophore (emission maximum at 665 nm, Figure 2, left) is considerably reduced at 20% dilution (Figure 2, middle) and becomes practically inactive at an 8% dilution (Figure 2).

Recent studies showed that CDs can have concentration-dependent luminescence, often with significant blue shifts.[89−92] For example, Meng et al.[89] reported a 200 nm shift (from 630 to 400 nm) in the PL emission peaks as their CDs' concentration gradually decreased from 3.0 to 0.03 g L^{-1}. In another study, Zhang et al.[90] communicated a shift from 678 to 435 nm for concentrations of 100 and 0.01 mg L^{-1},

https://doi.org/10.1021/acsnanoscienceau.4c00048
ACS Nanosci. Au XXXX, XXX, XXX−XXX

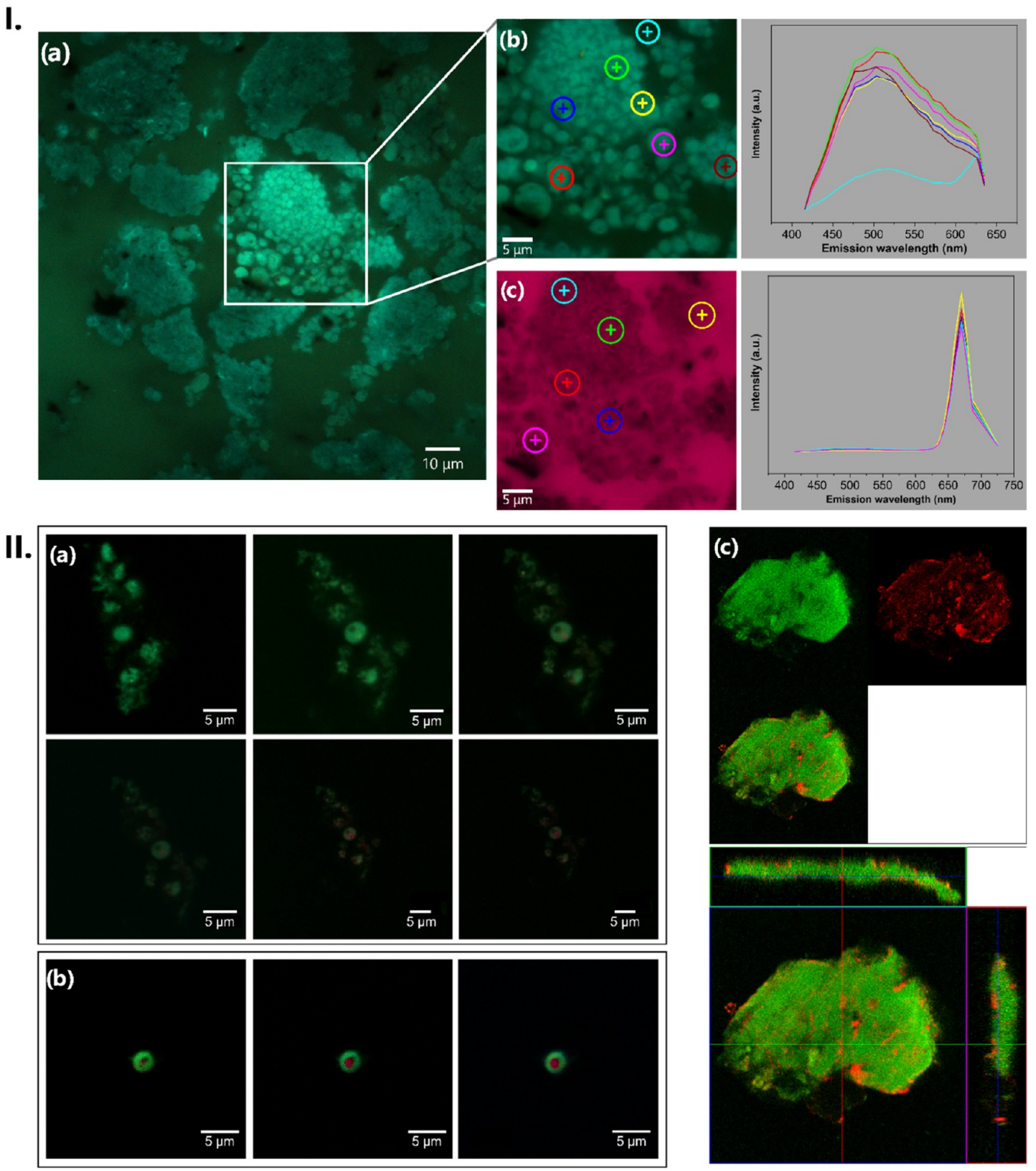

Figure 3. Representative confocal microscopy images of fluorometric analysis of (I) the *C. pyrenoidosa* extract: (a) fluorometric analysis with a solid-state laser exciting at 405 nm; (b) expansion of the previous image with an excitation wavelength of 405 nm and the corresponding fluorescence emission profile, obtained at several points in the image; (c) same expansion as in panel (b), now under an excitation wavelength of 633 nm with the corresponding fluorescence profile. (II) The CDCS aqueous solution: (a) under a laser exciting at 405 nm (10%) and 633 nm at different confocal distances; (b) under a laser exciting at 405 and 633 nm, with intensities of 10 and 100%, respectively, also at different confocal distances; (c) above: fluorescence images acquired under different channels (488 nm in the left and 633 nm in the right) as well as the reconstructed z-stack images (in the middle); below: the orthogonal view of the reconstructed image from z-stack images (built from a total of 35 images).

respectively. In these[89,90] and other studies,[91−93] the effect was attributed to an increase in the CDs' interparticle distance, leading to a disaggregation effect. Thus, for high concentrations, the formation of CD-aggregates helps stabilize the

https://doi.org/10.1021/acsnanoscienceau.4c00048
ACS Nanosci. Au XXXX, XXX, XXX−XXX

solution by minimizing the instability caused by the CDs' short distance and the high surface energy. Upon dilution, these aggregates break apart due to intermolecular interactions.[89,92]

Such an effect could very well be at play here. The CDs' PL properties might indeed be concentration-dependent, and the shift observed from green to blue emission might be a consequence of particle disaggregation due to dilution.[92] On the other hand, water addition also leads to a loss of emission of the Chl centers and, thus, of any synergy between these two phosphors. If that is the case, then introducing more solvent will make the PL properties of the CDCS closer to those of the CDs themselves. Nevertheless, the maximum Φ values found for the water-based solutions were 0.02 ± 0.01, independently of the concentration of CDs (Table S4 in Supporting Information).

3.4. Colorant Profile

The presence of Chl in our final systems justified further studies. When considering the whole process of CDs' formation, where *C. pyrenoidosa* biomass is exposed to a very acidic solvent and a MW treatment, the presence of Chl seems unlikely. Chls are quite stable in their natural environment, but they can easily degrade during extraction and processing steps due to exposure to heat, light, acids, oxygen, or enzymes.[94,95] In particular, chemical environments with low value of pH have been associated with the loss of the central Mg^{2+} cation, followed by the incorporation of protons to form pheophytin and the resulting change of color from bright green to olive green (Figure S12 in Supporting Information).[96,97] Likewise, thermal treatment can also lead to the replacement of the chelated Mg^{2+} cation, with additional exposure to either heat or acid resulting in the loss of the phytol chain attached to the porphyrin ring, thus forming a pheophorbide (Figure S12).[98,99] Of note, even though these compounds are structurally different, their absorption spectra are quite similar.[83,86,99] Both heat and acids were used in the formation process of CDs, and for this reason, the band ascribed to Chl in the UV−vis absorption spectra may indicate, instead of Chl itself, the presence of one (or more) of its degradation products.

In our experiments, we managed to extract Chl from the cells of *C. pyrenoidosa*. The spectrophotometric determination of the total Chl content was about 0.9 mg $mL_{extract}^{-1}$, corresponding to 9 mg of $g_{dried\ C.\ pyrenoidosa}^{-1}$. This result is a considerable improvement over the one recently reported by Ozel et al.,[68] of 21.49 ± 0.42 mg $L_{extract}^{-1}$ for the total Chl content extracted from *Chlorella vulgaris* with an AA/ChCl (2:1) ES. However, spectrophotometric analysis was unable to determine the Chl content in the CDCS samples at the end of the process under the same experimental conditions. This is likely because of the prolonged contact between Chl and AA without any other component that might help stabilize the pigment, such as carbohydrates, which are known to increase the stability of natural pigments.[100,101] Moreover, the complexity of the CDCS prevented any further analysis, thereby hindering the possibility of deeper characterization to identify the specific colorant in the solution.

The presence of the Chl colorant in the CDCS further prompted us to replicate our CDs results using only a Chl extract instead of the whole *C. pyrenoidosa* extract. The resulting system did not exhibit any spectroscopic evidence (Figure S13−II in the Supporting Information) of Chl presence, thus confirming that this colorant was fully consumed in the carbonization process. Instead, a significant presence of nanostructures with an average diameter of 5.6 ± 1.7 nm was observed (Figure S13−I). While their shape was not perfectly circular, the presence of lattice fringes with a *d*-spacing of 0.21 nm—corresponding to the (100) diffraction plane of graphitic carbon—along with the dimensions of the structures, tally well with the formation of CDs.[73] Hence, if the Chl that we have in our extract does not survive the MW stage on its own, its presence needs to be explained in another way. This led to the hypothesis that Chl might be encapsulated or otherwise related to the excess *Chlorella* cells identified by the TGA results. Therefore, the decision was made to probe the biomass extract and the resulting CDCS solution directly using CM.

Figure 3-I shows that there is still a significant number of aggregates composed of ellipsoidal structures after the end of the extraction process. These structures, with dimensions ranging between 2 and 5 μm, were identified as unprocessed *C. pyrenoidosa* cells, as their dimensions and shape fit with what is seen in electronic microscopy for this microalga.[65−67] This result confirms what was first seen in the TGA measurements for the algae residue, demonstrating that the amount of *C. pyrenoidosa* used was higher than the amount that the AA/ChCl (16:1) solvent could effectively degrade. In addition, the fluorescence spectrum profile under excitation at 405 nm (Figure 3-Ib) shows a broad band peaking at 503 nm for all spherical objects, which is also in line with the emission spectrum of a cellular wall. However, when the sample was excited at 633 nm (Figure 3-Ic), the only observed spectrum was that of Chl, regardless of the monitored region. This means that the Chl dye is present not only in the cells but mostly in the solution, attesting that there was, at least, a partial extraction.

Confocal images of CDCS (Figure 3-II), in turn, reveal an entirely different situation. Although the whole *C. pyrenoidosa* cells were still visible (Figure 3-IIa,b), cell wall fragments were also clearly discerned (Figure 3-IIa,c). This means that some of the cells that were unaffected by the solvent were able to withstand the MW step, thus surviving the whole process. Additionally, Chl was only detected inside the whole cells (Figure 3-IIa,b) and on a few specific fragments (Figure 3-IIc; and Supporting Video 1), where it remained attached to the wall fragments. In conclusion, the source of Chl is the surviving *C. pyrenoidosa* whole cells and is a direct consequence of the high solid−liquid ratio of the mass of *C. pyrenoidosa* and the volume of AA/ChCl (16:1) used in these experiments.

This result is interesting because it shows that microalgae can withstand MW treatment. The implications seem quite clear: preserving the Chl pigments (and possibly other colorants) is possible, even under harsh experimental conditions, as long as the microalgae's cell wall remains intact throughout the entire treatment process. Although, such a process is restricted to unicellular organisms, it nevertheless remains an original and useful strategy that can be expanded to other species containing colorants of interest. More importantly, this process opens an enticing fresh take on the preparation of multiphosphor materials with in situ generated CDs in a simple, easy way.

3.5. Water−PEG Mixtures

To further understand the phenomena of the dependency of the CDCS' PL solution properties with the concentration—and in an attempt to restore its initial properties—weighted amounts of PEG-200 were consecutively added to the aqueous

https://doi.org/10.1021/acsnanoscienceau.4c00048
ACS Nanosci. Au XXXX, XXX, XXX−XXX

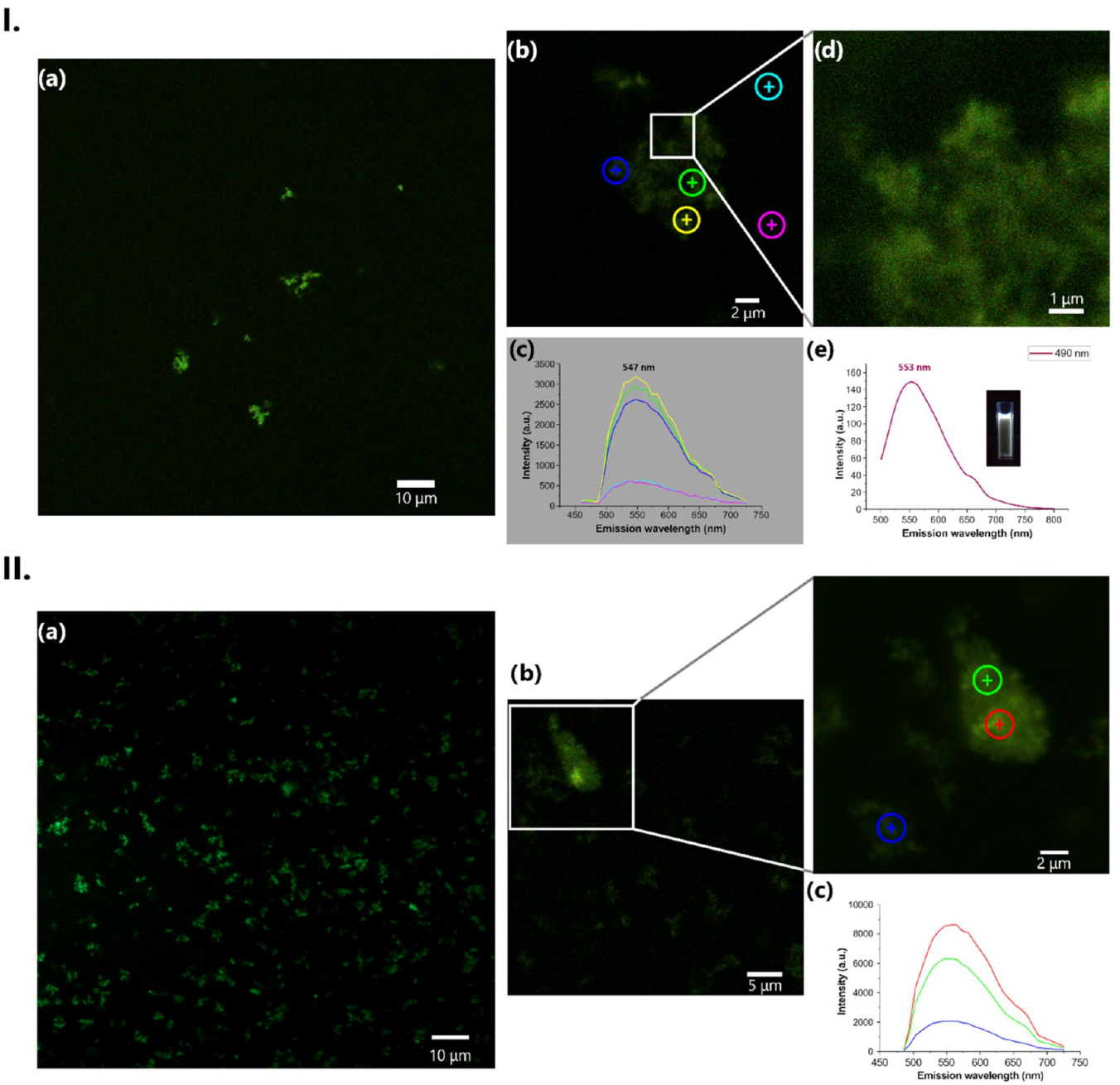

Figure 4. Representative confocal microscopy images of fluorometric analysis of (I) the 75% PEG-200 CDCS aqueous solution: (a) fluorometric analysis with a solid-state laser exciting at 488 nm; (b) expansion of image (a); (c) corresponding fluorescence emission profile, obtained at several points in (b); (d) expansion of image (b); and (e) fluorescence emission profile obtained for image (d) for excitation at 490 nm. (II) The CDCS PEG-200 solution: (a) under a laser exciting at wavelengths of 405 nm (25%) and 633 nm (100%); (b) expansion of the previous image under a laser exciting at 488 nm, and (c) fluorescence emission profile of image (b).

solution, and their optical properties were assessed ((3) in Scheme 1). The choice of PEG-200 as a cosolvent was guided by several reasons: it is in a liquid form at room temperature, has high polarizability, and demonstrates excellent solubility in water throughout all composition ranges.[102] Although, for a long time, PEG was deemed nonemissive—due to the lack of conjugated π systems or fluorophores—recent studies reported some rather interesting PL properties.[60,61,103] Such nonconjugated polymers self-assemble/aggregate in solution (normally for high concentrations) and in the solid state, yielding membranes and films. In the aggregated state, the oxygen atoms get together, favoring through-space delocalization of the lone pairs of electrons, and the rigid structure reduces nonradiative processes. The process—known as aggregation-induced emission—enables discrete chromophores or auxchromophores to engage in spatial conjugation via cooperative conformation (intramolecular) followed by aggregation (intermolecular), resulting in fluorescence or sometimes phosphorescence emission.[61,104]

The UV−vis absorption spectrum of PEG-200 shows a broad absorption band below 210 nm with a tail extending to 350 nm. Small shoulders are also seen at 262, 270, and 286 nm (Figure S14a in Supporting Information). The excitation spectrum of PEG-200 displays two distinct peaks centered at

https://doi.org/10.1021/acsnanoscienceau.4c00048
ACS Nanosci. Au XXXX, XXX, XXX−XXX

229 and 277 nm. Under radiation between 220 and 320 nm, the emission spectrum exhibits broad bands between 300 and 350 nm, with a tail extending to 500 nm. Irradiation at 230 nm led to the highest emission intensity at 305 nm, with the second highest emission occurring at 280 nm (Figure S14b,c). Sun et al.[61] reported similar spectra for PEG entities over a wide range of M_W (between 2 and 12 kDa), which agrees with those discussed here. Significantly, a red shift of the emission maxima was observed with increasing M_W (from 313 to 345 nm, corresponding to M_W values of 2 and 10 kDa, respectively). Thus, the maximum blue-shift now observed PEG-200 aligns with what would be expected for a low-M_W PEG. However, the PL properties of PEG are still open to debate, with a recent paper highlighting that the presence of fluorogenic stabilizers (i.e., 3-*tert*-butyl-4-hydroxyanisole, 3-BHA) in commercially available PEG products might be responsible for the recently discovered PL properties of PEG.[103] Indeed, the UV−vis absorption spectra of 3-BHA reported by Bin et al.[105] are very similar to the one we obtained for PEG-200, with absorption peaks at 223 and 278−280 nm that coincide with the excitation bands reported here.[103,105] Since the presence of 3-BHA in our PEG-200 cannot be excluded, any interpretation of the PL properties of PEG-200 should be taken with extreme care.

The PL properties of the CDCS solubilized in water/PEG mixtures over the whole PEG weight/molar fraction ranges are summarized in Table S3 (Supporting Information) and are represented in Figures S15−S17 (Supporting Information). The addition of small amounts of PEG to the aqueous CDCS solution primarily affects the fluorescence intensity, along with slight red shifts in both the excitation and emission maxima. This implies that the addition of PEG-200 to the system has an impact on the quenching of the fluorescence mechanisms. Even so, a PEG weight ratio of 75% or higher results in a pronounced increase in intensity, as well as a significant blue shift in the wavelength maxima (from 457 and 525 to 383 and 464 nm, for the excitation and the emission maxima, respectively). These concentration-dependent shifts indicate direct interactions between PEG oligomers and the surface of the CDCS fluorophores, supporting the presence of emissive surface states. The implication is that PEG-200 not only acts as a passivating agent in preventing particle aggregation but also modulates the PL properties of the CDCS. Despite that, there are no significant changes in the Φ values of the water/PEG-200 mixtures to those of the only water or only PEG-200 solvent, the maximum value being 0.02 ± 0.01 (Table S4, Supporting Information).

Several studies reported negative deviations of excess molar volumes of water/low-M_W PEG mixtures, indicating a volume contraction upon mixing.[106−109] This effect was correlated with a 3D H-bonded structure arising from the interactions between water and the PEG molecules within the mixture. In the case of PEG-200, these intermolecular H-bonding interactions attained a maximum at a PEG molar fraction, $\chi_{PEG} \approx 0.26$ (which corresponds to about 80% wt PEG), regardless of the temperature.[107−109] The major contribution to the significant negative excess molar volumes of the mixture was attributed to the H-bonding between the water − O− and the terminal − H of PEG. The presence of weaker H-bonding interactions between the water − H and the ether − O− of PEG, however, cannot be discarded. Thus, small additions of PEG-200 are expected to bring some heterogeneities to the solution but without significant changes to the environment around the fluorophores, which seems to fit the small variations observed in the intensity and the position of the Chl and the CDs bands (Figures S16 and S17). Borodin et al.[110] studied the polymer dynamics of aqueous PEG solutions and found that the first hydration shell is largely formed for an aqueous PEG solution at 50%. Although their study focused on PEG-600, it has been shown that variation in hydration numbers for PEG-200 and PEG-600 was minimal (6.06 and 5.76, respectively).[111] As illustrated in Table S3 and Figure S15, the PL properties of the CDCS in water/PEG-200 solutions for a weight ratio below 60% remain relatively stable despite gradual intensity increases due to the formation of H-bonding networks between H_2O and PEG-200. At about 75−80% PEG-200 weight ratio, the interactions with H_2O are at their strongest, followed by a stage where PEG-rich areas begin to form at higher PEG-200 weight ratios.[107−110] At this stage, there is a notable blue shift in excitation and emission maxima (from 457 and 525 nm to 383 and 464 nm, respectively), resembling the shift seen when the CDCS is diluted in water. This observation hints at a diminishing influence of Chl, potentially indicating some synergy between the CDs and the *C. pyrenoidosa* cells.

The CM images obtained for the 75% PEG-200 aqueous solution and 100% PEG-200 solutions of CDCS are represented in Figure 4. As observed, no Chl was detected in either solution. In both cases, only small structures were found, closely resembling fragments. These structures were more common in the full 100% PEG-200 solution than in the 75% PEG-200 solution (Figure 4-I,II, respectively). Upon magnification, emission profiling was performed for the selected areas. A peak was observed at around 547−557 nm (Figures 4-Ic,IIc), coinciding with the emission spectra for the CDCS solution under excitation at 490 nm (Figure 4-Id), which led to its attribution to CD clusters. Moreover, a second set of structures was found in the 75% PEG-200 aqueous solution, with profiling revealing a band centered at 511 nm after excitation at 405 nm (Figure S18 in the Supporting Information). Given the resemblance of the spectrum obtained here (Figure S18) with that of the *C. pyrenoidosa* extract (Figure 3-Ib), we interpreted these second structures as cell wall fragments because these are the only visible structures observable in the *C. pyrenoidosa* extract.

The absence of whole cells of *C. pyrenoidosa* in both solutions made us hypothesize that they suffer lysis upon dispersion in PEG-rich solutions. This may explain the consistent loss of intensity of the Chl Q-band in the emission spectra, as the PEG-200:water ratio increased (Figures S16 and S17). The foundations for our hypothesis are based on two concomitant mechanisms of action. First, PEG is known to interact with cell walls and alter their plasticity and permeability, rendering them more susceptible to osmotic pressure.[112,113] Second, the osmotic stress induced by introducing high concentrations of PEG-200 to the aqueous solution contributed to the damage in the cell wall, eventually leading to cell disruption.[114] Even so, by introducing small quantities of PEG-200, it remains possible to fine-tune the PL properties of the CDCS, which could be advantageous for designing the active layer of LSCs.

3.6. Luminescent Solar Concentrators (LSCs)

Planar LSCs were fabricated from CDCS-in-water and CDCS-in-100% PEG-200 samples. Each solution was used to fill a glass container coupled to a c-Si PV cell, as previously

https://doi.org/10.1021/acsnanoscienceau.4c00048
ACS Nanosci. Au XXXX, XXX, XXX−XXX

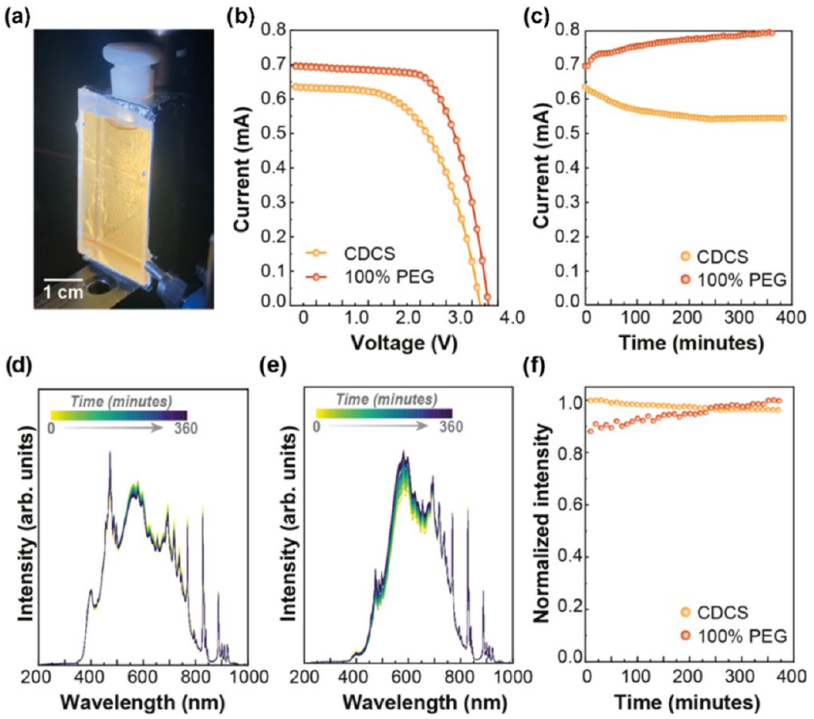

Figure 5. Luminescent solar concentrator (LSC). (a) Photograph of the fabricated LSC based on the CDCS-in-water sample under simulated AM1.5G irradiation. (b) *I*–*V* curves and (c) measured short-circuit current values during continuous exposure to AM1.5G irradiation. Emission spectra measured at the edges of the LSCs are shown for (d) the CDCS-in-water sample and (e) the CDCS-in-100% PEG sample, both under AM1.5G irradiation. (f) Variation in the integrated area of emission spectra over the exposure time.

reported.[19] Each device was characterized under simulated AM1.5G irradiation (Figure 5a), and the conversion efficiency ($\eta_{opt} = P_{out}/P_{in}$, where P_{out} is the output optical power and P_{in} is the incident optical power) and power conversion efficiency (PCE = P_{out}^{el}/P_{in}, where P_{out}^{el} is the electrical output power) were calculated following standard methods[115] (see the Supporting Information for details). The CDCS-in-water-based device yielded η_{opt} and PCE values of 9.4 ± 0.3 and 0.17 ± 0.01%, respectively, while the LSC based on the CDCS-in-100% PEG-200 sample reached η_{opt} and PCE values of 10.7 ± 0.4 and 0.23 ± 0.01%. This indicates no significant difference between the water and PEG-200 media (Figure 5b). Comparing the performance[75] with other CDs and natural-based centers (Table S5), it is possible to infer that the results here reported are among the best ones. To test the performance in a time-extended operation mode, the fabricated LSC devices were exposed continuously to AM1.5G radiation for 6 h, retaining approximately 90% of their initial electrical (Figure 5c) and optical (Figure 5d–f) performance for the CDCS. For the PEG-200-based LSCs, the electrical current and the intensity that showed an initial increase were stable during the experiment, in good agreement with the PEG-200 acting as a protective layer for the CDs. The spectra reported show the solar simulator output modified by the LSCs' absorption and emission, confirming their capability to absorb and convert solar radiation.

4. CONCLUSIONS

In this work, CDs have been prepared from *C. pyrenoidosa* biomass, obtained from a commercial source through MW carbonization. For this process, an ES consisting of AA and ChCl was used as the extracting agent and solvent medium. The resulting CDs, with a diameter of 3.9 ± 0.7 nm, exhibit emission in the green region of the spectrum (526 nm) upon excitation in the blue region (472 nm). More interestingly, this procedure also retained Chl centers, emitting in the far-red region of the spectrum. These Chl centers are due to the presence of *C. pyrenoidosa* cells, which managed to survive both the extraction and the MW procedures due to the high solid–liquid ratio, meaning the mass of *C. pyrenoidosa* per mL of ES used in the procedure, making this system a two-phosphor system emitting in the green and red regions. Additionally, there seems to be a synergistic effect between these two phosphors since the CD PL properties are blue-shifted whenever the activity of the chlorophyllin centers diminishes, either through dilution or by introducing a high concentration of PEG-200 oligomers. Overall, introducing PEG-200 entities also led to an improved PL system, evidenced by increased fluorescence intensity and narrowed excitation and emission bands, particularly PEG-200/water ratios up to 75%. When placed in a planar LSC cell, the CDCS-in-100%PEG-200 revealed photostability and optical and power conversion efficiency values of 11 and 0.2%, respectively, comparable to state-of-the-art CDs-based LSCs.

■ ASSOCIATED CONTENT

Supporting Information

The Supporting Information is available free of charge at https://pubs.acs.org/doi/10.1021/acsnanoscienceau.4c00048.

Results for DSC and FTIR (for the eutectic system); ATR-FTIR, as well as additional thermogravimetric analyses, TEM, and PL measurements for the CDCS system and the control experiment performed for the Chl extract; and additional PL measurements for the CDCS in water/PEG-200 solutions (PDF)

https://doi.org/10.1021/acsnanoscienceau.4c00048
ACS Nanosci. Au XXXX, XXX, XXX–XXX

Video animation of the z-stack images obtained for the CDCS system by CM (AVI)

AUTHOR INFORMATION

Corresponding Author

Filipe M. Santos − *Fiber Materials and Environmental Technologies (FibEnTech-UBI), Universidade da Beira Interior, 6201-001 Covilhã, Portugal;* orcid.org/0000-0001-9370-0919; Email: filipe.miguel.santos@ubi.pt

Authors

Tiago A. G. Duarte − *CQ-VR, Universidade de Trás-os-Montes e Alto Douro, 5000-801 Vila Real, Portugal;* orcid.org/0000-0003-3774-5842

Sandra F. H. Correia − *Instituto de Telecomunicações, Universidade de Aveiro, 3810-193 Aveiro, Portugal;* orcid.org/0000-0002-6851-6041

Rui F. P. Pereira − *Centre of Chemistry, Universidade do Minho, 4710-057 Braga, Portugal;* orcid.org/0000-0001-7279-5728

Alexandra Conde − *Departamento de Química, CICECO—Aveiro Institute of Materials, Universidade de Aveiro, 3810-193 Aveiro, Portugal*

Álvaro R. Ribeiro − *CQ-VR, Universidade de Trás-os-Montes e Alto Douro, 5000-801 Vila Real, Portugal*

Susana Santos Braga − *LAQV-REQUIMTE, Departmento de Química, Universidade de Aveiro, 3810-193 Aveiro, Portugal;* orcid.org/0000-0003-4460-970X

Sónia P. M. Ventura − *Departamento de Química, CICECO—Aveiro Institute of Materials, Universidade de Aveiro, 3810-193 Aveiro, Portugal;* orcid.org/0000-0001-9049-4267

Rute A. S. Ferreira − *Departmento de Física, CICECO—Aveiro Institute of Materials, Universidade de Aveiro, 3810-193 Aveiro, Portugal;* orcid.org/0000-0003-1085-7836

Verónica de Zea Bermudez − *CQ-VR, Universidade de Trás-os-Montes e Alto Douro, 5000-801 Vila Real, Portugal; CQ-VR, Universidade de Trás-os-Montes e Alto Douro, 5000-801 Vila Real, Portugal;* orcid.org/0000-0002-7577-4938

Sílvia C. Nunes − *Fiber Materials and Environmental Technologies (FibEnTech-UBI), Universidade da Beira Interior, 6201-001 Covilhã, Portugal; Departamento de Química, Universidade da Beira Interior, 6201-001 Covilhã, Portugal;* orcid.org/0000-0001-8993-3162

Complete contact information is available at: https://pubs.acs.org/10.1021/acsnanoscienceau.4c00048

Author Contributions

[¶]T.A.G.D., S.F.H.C., and R.F.P.P. have contributed equally to this work. The manuscript was written through contributions of all authors. All authors have given approval to the final version of the manuscript. CRediT: **Filipe M. Santos** conceptualization, data curation, formal analysis, investigation, methodology, visualization, writing - original draft, writing - review & editing; **Tiago A. G. Duarte** data curation, formal analysis, visualization, writing - original draft, writing - review & editing; **Sandra F.H. Correia** formal analysis, investigation, methodology, visualization, writing - review & editing; **Rui F. P. Pereira** data curation, formal analysis, investigation, methodology, visualization, writing - original draft, writing - review & editing; **Alexandra Conde** formal analysis; **Álvaro R. Ribeiro** formal analysis, investigation; **Susana Santos Braga** data curation, formal analysis, investigation, resources, writing - original draft, writing - review & editing; **Sónia P.M. Ventura** formal analysis, investigation, methodology, supervision, writing - original draft, writing - review & editing; **Rute A.S. Ferreira** formal analysis, funding acquisition, project administration, supervision, writing - review & editing; **Verónica de Zea Bermudez** funding acquisition, methodology, project administration, resources, supervision, visualization, writing - original draft, writing - review & editing; **Sílvia C. Nunes** data curation, formal analysis, investigation, project administration, resources, supervision, writing - original draft, writing - review & editing.

Funding

This study was financed by the project A-MoVeR− 'Mobilizing Agenda for the Development of Products & Systems toward an Intelligent and Green Mobility,'' operation No. 02/C05-i01.01/2022.PC646908627−00000069, approved under the terms of the call No. 02/C05-i01/2022−Mobilizing Agendas for Business Innovation, financed by European funds provided to Portugal by the Recovery and Resilience Plan (RRP), in the scope of the European Recovery and Resilience Facility (RRF), framed in the Next Generation UE, for the period of 2021−2026. The authors acknowledge thesupport by national funds from the Foundation for Science and Technology (FCT) and SOLPOWINS (PTDC/CTM-REF/4304/2020). This research wasdeveloped within the scope of the projects Fiber Materials and Environmental Technologies (FibEnTech-UBI) (UIDB/00195/2020 (DOI: 10.54499/UIDB/00195/2020)), Centro de Quimica-Vila Real (CQ-VR) (UIDB/00616/2020 (DOI: 10.54499/UIDB/00616/2020) and UIDP/00616/2020 (DOI: 10.54499/UIDP/00616/2020)), CICECO-Aveiro Institute of Materials UIDB/50011/2020 (DOI: 10.54499/UIDB/50011/2020), UIDP/50011/2020 (DOI: 10.54499/UIDP/50011/2020) & LA/P/0006/2020 (DOI: 10.54499/LA/P/0006/2020), CQ-UM (UIDB/00686/2020 (DOI: 10.54499/UIDB/00686/2020) and UIDP/00686/2020 (DOI: 10.54499/UIDP/00686/2020)) and Instituto de Telecomunicações (UIDB/50008/2020 (DOI: 10.54499/UIDB/50008/2020), UIDP/50008/2020 (DOI: 10.54499/50008/2020) and LA/P/0109/2020 (DOI: 10.54499/LA/P/0109/2020)),financed by national funds through the FCT/MCTES (PIDDAC). LAQV-REQUIMTE (ref UIDB/50006/2020, DOI: 10.54499/UIDP/50006/2020) acknowledges funding by FCT/MCTES through national funds (PIDDAC) and, where applicable, cofinanced by the European Regional Development Fund (FEDER). F.M.S. acknowledges the SOLPOWINS project for his Junior Research contract. S.C.N. and R.F.P.P. acknowledge the FCT for the Assistant Research contracts (https://doi.org/10.54499/2020.00805.CEECIND/CP1625/CT0001 and 2023.07994.CEECIND, respectively) and S.F.H.C. also acknowledges the FCT for the Junior Research Contract (2022.03740.CEECIND/CP1716/CT0006) in the scope of Scientific Employment Stimulus.

Notes

The authors declare no competing financial interest.

ACKNOWLEDGMENTS

Prof. Artur J. Valente (Universidade de Coimbra) is acknowledged for the DSC measurement. Celeste Azevedo (UA) is acknowledged for last-minute thermogravimetric measurements. Gonçalo Sobral (UTAD) is acknowledged for his

help with the synthetic procedures. This work was carried out in part through the use of the INL User Facilities.

ABBREVIATIONS

AA, acetic acid; AA: ChCl, acetic acid: cholinium chloride solvent; ATR-FTIR, attenuated total reflectance Fourier transformed Infrared; BIPV, building-integrated photovoltaics; CD, carbon dots; CDCS, carbon dots/chlorophyll system; CDS, solvent-derived carbon dots; Ch+, cholinium cation; ChCl, cholinium chloride; Chl, chlorophyll; CM, confocal microscopy; DSC, differential scanning calorimetry; DTGA, first-derivative of the TGA; ES, eutectiv solvent; HBA, hydrogen bond acceptor; HBD, hydrogen bond donor (HBD); MW, molecular weight; HR-TEM, high-resolution transmission electron microscopy; PEG-200, poly(ethylene glycol) with a molecular weight of 200; PL, photoluminescence; PV, photocoltaic; TGA, thermogravimetric analysis; UV−vis, UV−visible absorption; spectra

REFERENCES

(1) Richards, B. S.; Howard, I. A. Luminescent solar concentrators for building integrated photovoltaics: opportunities and challenges. *Energy Environ. Sci.* **2023**, *16*, 3214−3239.
(2) Meinardi, F.; Bruni, F.; Brovelli, S. Luminescent solar concentrators for building-integrated photovoltaics. *Nat. Rev. Mater.* **2017**, *2*, No. 17072.
(3) Figueiredo, G.; Correia, S. F. H.; Falcão, B. P.; Sencadas, V.; Fu, L.; André, P. S.; Ferreira, R. A. S. Multi-surface adhesion luminescent solar concentrators for supply-less IoT. *Adv. Sci.* **2024**, *11*, No. 2400540.
(4) Ferreira, R. A. S.; Correia, S. F. H.; Monguzzi, A.; Liu, X.; Meinardi, F. Spectral converters for photovoltaics − what's ahead. *Mater. Today* **2020**, *33*, 105−121.
(5) Correia, S. F. H.; de Zea Bermudez, V.; Ribeiro, S. J. L.; André, P. S.; Ferreira, R. A. S.; Carlos, L. D. Luminescent solar concentrators: challenges for lanthanide-based organic−inorganic hybrid materials. *J. Mater. Chem. A* **2014**, *2*, 5580−5596.
(6) Figueiredo, G.; Correia, S. F. H.; Fu, L.; de Zea Bermudez, V.; Neto, A. N. C.; André, P. S.; Ferreira, R. A. S. Luminescent Solar Concentrators: Current and Future Applications in Smart Cities. In *Handbook on the Physics and Chemistry of Rare Earths*; Bünzli, J.-C.; Kauzlarich, S. M., Eds.; Elsevier, 2024; Vol. *66*.
(7) Hernández-Rodríguez, M. A.; Correia, S. F. H.; Ferreira, R. A. S.; Carlos, L. D. A perspective on sustainable luminescent solar concentrators. *J. Appl. Phys.* **2022**, *131*, No. 140901.
(8) Li, J.; Zhao, H.; Zhao, X.; Gong, X. High-efficiency luminescent solar concentrators based on carbon dots with simultaneously ultrabright solid-state and liquid-state luminescence. *Adv. Funct. Mater.* **2024**, *34*, No. 2404473.
(9) Arrigo, A.; Cancelliere, A. M.; Galletta, M.; Burtone, A.; Lanteri, G.; Nastasi, F.; Puntoriero, F. From waste to energy: luminescent solar concentrators based on carbon dots derived from surgical facemasks. *Mater. Adv.* **2023**, *4*, 5200−5205.
(10) Zhou, Y.; Benetti, D.; Tong, X.; Jin, L.; Wang, Z. M.; Ma, D.; Zhao, H.; Rosei, F. Colloidal carbon dots based highly stable luminescent solar concentrators. *Nano Energy* **2018**, *44*, 378−387.
(11) Hu, C.; Li, M.; Qiu, J.; Sun, Y.-P. Design and fabrication of carbon dots for energy conversion and storage. *Chem. Soc. Rev.* **2019**, *48*, 2315−2337.
(12) Đorđević, L.; Arcudi, F.; Cacioppo, M.; Prato, M. A multifunctional chemical toolbox to engineer carbon dots for biomedical and energy applications. *Nat. Nanotechnol.* **2022**, *17*, 112−130.
(13) Zhao, H.; Liu, G.; You, S.; Camargo, F. V. d. A.; Zavelani-Rossi, M.; Wang, X.; Sun, C.; Liu, B.; Zhang, Y.; Han, G.; Vomiero, A.; Gong, X. Gram-scale synthesis of carbon quantum dots with a large Stokes shift for the fabrication of eco-friendly and high-efficiency luminescent solar concentrators. *Energy Environ. Sci.* **2021**, *14*, 396−406.
(14) Ren, J.; Opoku, H.; Tang, S.; Edman, L.; Wang, J. Carbon dots: a review with focus on sustainability. *Adv. Sci.* **2024**, *11*, No. 2405472.
(15) Sharma, A.; Das, J. Small molecules derived carbon dots: synthesis and applications in sensing, catalysis, imaging, and biomedicine. *J. Nanobiotechnol.* **2019**, *17*, No. 92.
(16) Meng, W.; Bai, X.; Wang, B.; Liu, Z.; Lu, S.; Yang, B. Biomass-derived carbon dots and their applications. *Energy Environ. Mater.* **2019**, *2*, 172−192.
(17) Rodrigues, A. V.; de Souza, D. A. R.; Garcia, F. D. R.; Ribeiro, S. J. L. Renewable energy for a green future: electricity produced from efficient luminescent solar concentrators. *Sol. Energy Adv.* **2022**, *2*, No. 100013.
(18) Frias, A. R.; Pécoraro, É.; Correia, S. F. H.; Minas, L. M. G.; Bastos, A. R.; García-Revilla, S.; Balda, R.; Ribeiro, S. J. L.; André, P. S.; Carlos, L. D.; Ferreira, R. A. S. Sustainable luminescent solar concentrators based on organic−inorganic hybrids modified with chlorophyll. *J. Mater. Chem. A* **2018**, *6*, 8712−8723.
(19) Correia, S. F. H.; Bastos, A. R. N.; Martins, M.; Macário, I. P. E.; Veloso, T.; Pereira, J. L.; Coutinho, J. A. P.; Ventura, S. P. M.; André, P. S.; Ferreira, R. A. S. Bio-based solar energy harvesting for onsite mobile optical temperature sensing in smart cities. *Adv. Sci.* **2022**, *9*, No. 2104801.
(20) Frias, A. R.; Correia, S. F. H.; Martins, M.; Ventura, S. P. M.; Pecoraro, E.; Ribeiro, S. J. L.; André, P. S.; Ferreira, R. A. S.; Coutinho, J. A. P.; Carlos, L. D. Sustainable liquid luminescent solar concentrators. *Adv. Sustainable Syst.* **2019**, *3*, No. 1800134.
(21) Fabris, M.; Abbriano, R. M.; Pernice, M.; Sutherland, D. L.; Commault, A. S.; Hall, C. C.; Labeeuw, L.; McCauley, J. I.; Kuzhiuparambil, U.; Ray, P.; Kahlke, T.; Ralph, P. J. Emerging technologies in algal biotechnology: toward the establishment of a sustainable, algae-based bioeconomy. *Front. Plant Sci.* **2020**, *11*, No. 279.
(22) Barbosa, M. J.; Janssen, M.; Südfeld, C.; D'Adamo, S.; Wijffels, R. H. Hypes, hopes, and the way forward for microalgal biotechnology. *Trends Biotechnol.* **2023**, *41*, 452−471.
(23) Olabi, A. G.; Shehata, N.; Sayed, E. T.; Rodriguez, C.; Anyanwu, R. C.; Russell, C.; Abdelkareem, M. A. Role of microalgae in achieving sustainable development goals and circular economy. *Sci. Total Environ.* **2023**, *854*, No. 158689.
(24) Borowitzka, M. A. Microalgae in Medicine and Human Health: A Historical Perspective. In *Microalgae in Health and Disease Prevention*; Levine, I. A.; Fleurence, J., Eds.; Academic Press, 2018; pp 195−210.
(25) Hassan, S.; Meenatchi, R.; Pachillu, K.; Bansal, S.; Brindangnanam, P.; Arockiaraj, J.; Kiran, G. S.; Selvin, J. Identification and characterization of the novel bioactive compounds from microalgae and cyanobacteria for pharmaceutical and nutraceutical applications. *J. Basic Microbiol.* **2022**, *62*, 999−1029.
(26) Chia, W. Y.; Tang, D. Y. Y.; Khoo, K. S.; Lup, A. N. K.; Chew, K. W. Nature's fight against plastic pollution: algae for plastic biodegradation and bioplastics production. *Environ. Sci. Ecotechnol.* **2020**, *4*, No. 100065.
(27) Chong, J. W. R.; Tan, X.; Khoo, K. S.; Ng, H. S.; Jonglertjunya, W.; Yew, G. Y.; Show, P. L. Microalgae-based bioplastics: future solution towards mitigation of plastic wastes. *Environ. Res.* **2022**, *206*, No. 112620.
(28) Jalilian, N.; Najafpour, G. D.; Khajouei, M. Macro and micro algae in pollution control and biofuel production − a review. *ChemBioEng Rev.* **2020**, *7*, 18−33.
(29) Nguyen, L. N.; Vu, M. T.; Vu, H. P.; Johir, M. A. H.; Labeeuw, L.; Ralph, P. J.; Mahlia, T. M. I.; Pandey, A.; Sirohi, R.; Nghiem, L. D. Microalgae-based carbon capture and utilization: A critical review on current system developments and biomass utilization. *Crit. Rev. Environ. Sci. Technol.* **2023**, *53*, 216−238.
(30) Choudhary, S.; Tripathi, S.; Poluri, K. M. Microalgal-based bioenergy: strategies, prospects, and sustainability. *Energy Fuels* **2022**, *36*, 14584−14612.

https://doi.org/10.1021/acsnanoscienceau.4c00048
ACS Nanosci. Au XXXX, XXX, XXX−XXX

(31) Torres, F. G.; De-la-Torre, G. E. Green algae as a sustainable source for energy generation and storage technologies. *Sustainable Energy Technol. Assess.* **2022**, *53*, No. 102658.
(32) Dolganyuk, V.; Belova, D.; Babich, O.; Prosekov, A.; Ivanova, S.; Katserov, D.; Patyukov, N.; Sukhikh, S. Microalgae: a promising source of valuable bioproducts. *Biomolecules* **2020**, *10*, No. 1153.
(33) Hachicha, R.; Elleuch, F.; Ben Hlima, H.; Dubessay, P.; de Baynast, H.; Delattre, C.; Pierre, G.; Hachicha, R.; Abdelkafi, S.; Michaud, P.; Fendri, I. Biomolecules from microalgae and cyanobacteria: applications and market survey. *Appl. Sci.* **2022**, *12*, No. 1924.
(34) Sandgruber, F.; Gielsdorf, A.; Baur, A. C.; Schenz, B.; Müller, S. M.; Schwerdtle, T.; Stangl, G. I.; Griehl, C.; Lorkowski, S.; Dawczynski, C. Variability in macro- and micronutrients of 15 commercially available microalgae powders. *Mar. Drugs* **2021**, *19*, No. 310.
(35) Chen, F.; Qian, J.; He, Y.; Leng, Y.; Zhou, W. Could Chlorella pyrenoidosa be exploited as an alternative nutrition source in aquaculture feed? A study on the nutritional values and anti-nutritional factors. *Front. Nutr.* **2022**, *9*, No. 1069760.
(36) Guo, D.; Lyu, Y.; Gao, Y.; Lin, Y.; Zhang, X.; Pan, Y.; Zhu, Y. Synthesis, solution and solid-state fluorescence of nitrogen self-doped carbon dots derived from Chlorella pyrenoidosa. *Colloids Surf., A* **2021**, *631*, No. 127741.
(37) Zhang, J.; Xia, A.; Chen, H.; Nizami, A.-S.; Huang, Y.; Zhu, X.; Zhu, X.; Liao, Q. Biobased carbon dots production via hydrothermal conversion of microalgae Chlorella pyrenoidosa. *Sci. Total Environ.* **2022**, *839*, No. 156144.
(38) Pena, A. C. C.; Raymundo, L. M.; Trierweiler, L. F.; Gutterres, M. Green carbon dots synthesized from Chlorella Sorokiniana microalgae biochar for chrome detection. *J. Ind. Eng. Chem.* **2023**, *117*, 130−139.
(39) Borzyszkowska, A. F.; Sulowska, A.; Czaja, P.; Bielicka-Giełdoń, A.; Zekker, I.; Zielińska-Jurek, A. ZnO-decorated green-synthesized multi-doped carbon dots from Chlorella pyrenoidosa for sustainable photocatalytic carbamazepine degradation. *RSC Adv.* **2023**, *13*, 25529−25551.
(40) Pôjo, V.; Tavares, T.; Malcata, F. X. Processing methodologies of wet microalga biomass toward oil separation: an overview. *Molecules* **2021**, *26*, No. 641.
(41) Bernaerts, T. M. M.; Gheysen, L.; Foubert, I.; Hendrickx, M. E.; Van Loey, A. M. The potential of microalgae and their biopolymers as structuring ingredients in food: A review. *Biotechnol. Adv.* **2019**, *37*, No. 107419.
(42) Guo, L.-P.; Zhang, Y.; Li, W.-C. Sustainable microalgae for the simultaneous synthesis of carbon quantum dots for cellular imaging and porous carbon for CO2 capture. *J. Colloid Interface Sci.* **2017**, *493*, 257−264.
(43) Dong, D.; Liu, T.; Liang, D.; Jin, X.; Qi, Z.; Li, A.; Ning, Y. Facile hydrothermal synthesis of chlorella-derived environmentally friendly fluorescent carbon dots for differentiation of living and dead Chlorella. *ACS Appl. Bio Mater.* **2021**, *4*, 3697−3705.
(44) Zha, Z.; Lai, J.; Li, Y.; Yang, J.; Cui, S.; Li, Y. The degradation of tetracycline by modified BiOCl nanosheets with carbon dots from the Chlorella. *J. Alloys Compd.* **2021**, *855*, No. 157454.
(45) Jafari, S. M.; Masoum, S.; Tafreshi, S. A. H. A microlagal-based carbonaceous sensor for enzymatic determination of glucose in blood serum. *J. Ind. Eng. Chem.* **2021**, *101*, 195−204.
(46) Wang, N.; Zheng, A.-Q.; Liu, X.; Chen, J.-J.; Yang, T.; Chen, M.-L.; Wang, J.-H. Deep eutectic solvent-assisted preparation of nitrogen/chloride-doped carbon dots for intracellular biological sensing and live cell imaging. *ACS Appl. Mater. Interfaces* **2018**, *10*, 7901−7909.
(47) Wang, M.; Li, C.; Zhou, M.; Xia, Z.; Huang, Y. Natural deep eutectic solvent assisted synthesis and applications of chiral carbon dots. *Green Chem.* **2022**, *24*, 6696−6706.
(48) Liu, S.; Quan, T.; Yang, L.; Deng, L.; Kang, X.; Gao, M.; Xia, Z.; Li, X.; Gao, D. N,Cl-codoped carbon dots from Impatiens balsamina L. stems and a deep eutectic solvent and their applications for gram-positive bacteria identification, antibacterial activity, cell imaging, and ClO− sensing. *ACS Omega* **2021**, *6*, 29022−29036.
(49) Chen, Y.; Mu, T. Application of deep eutectic solvents in biomass pretreatment and conversion. *Green Energy Environ.* **2019**, *4*, 95−115.
(50) del Mar Contreras-Gámez, M.; Galán-Martín, Á.; Seixas, N.; da Costa Lopes, A. M.; Silvestre, A.; Castro, E. Deep eutectic solvents for improved biomass pretreatment: Current status and future prospective towards sustainable processes. *Bioresour. Technol.* **2023**, *369*, No. 128396.
(51) Martins, M. A. R.; Pinho, S. P.; Coutinho, J. A. P. Insights into the nature of eutectic and deep eutectic mixtures. *J. Solution Chem.* **2019**, *48*, 962−982.
(52) Afonso, J.; Mezzetta, A.; Marrucho, I. M.; Guazzelli, L. History repeats itself again: Will the mistakes of the past for ILs be repeated for DESs? From being considered ionic liquids to becoming their alternative: the unbalanced turn of deep eutectic solvents. *Green Chem.* **2023**, *25*, 59−105.
(53) Abranches, D. O.; Coutinho, J. A. P. Everything you wanted to know about deep eutectic solvents but were afraid to be told. *Annu. Rev. Chem. Biomol. Eng.* **2023**, *14*, 141−163.
(54) Choi, Y. H.; van Spronsen, J.; Dai, Y.; Verberne, M.; Hollmann, F.; Arends, I. W. C. E.; Witkamp, G.-J.; Verpoorte, R. Are natural deep eutectic solvents the missing link in understanding cellular metabolism and physiology? *Plant Physiol.* **2011**, *156*, 1701−1705.
(55) Liu, Y.; Friesen, J. B.; McAlpine, J. B.; Lankin, D. C.; Chen, S.-N.; Pauli, G. F. Natural deep eutectic solvents: properties, applications, and perspectives. *J. Nat. Prod.* **2018**, *81*, 679−690.
(56) Brody, S. S.; Brody, M. Fluorescence properties of aggregated chlorophyll in vivo and in vitro. *Trans. Faraday Soc.* **1962**, *58*, 416−428.
(57) Murata, N.; Nishimura, M.; Takamiya, A. Fluorescence of chlorophyll in photosynthetic systems III. Emission and action spectra of fluorescence—Three emission bands of chlorophyll a and the energy transfer between two pigment systems. *Biochim. Biophys. Acta, Biophys. Incl. Photosynth.* **1966**, *126*, 234−243.
(58) Hoffmann, M. M. Polyethylene glycol as a green chemical solvent. *Curr. Opin. Colloid Interface Sci.* **2022**, *57*, No. 101537.
(59) Peng, Z.; Ji, C.; Zhou, Y.; Zhao, T.; Leblanc, R. M. Polyethylene glycol (PEG) derived carbon dots: preparation and applications. *Appl. Mater. Today* **2020**, *20*, No. 100677.
(60) Paik, S. P.; Ghatak, S. K.; Dey, D.; Sen, K. Poly(ethylene glycol) vesicles: self-assembled site for luminescence generation. *Anal. Chem.* **2012**, *84*, 7555−7561.
(61) Sun, C.; Jiang, X.; Li, B.; Li, S.; Kong, X. Z. Fluorescence behavior and mechanisms of poly(ethylene glycol) and their applications in Fe3+ and Cr6+ detections, data encryption, and cell imaging. *ACS Sustainable Chem. Eng.* **2021**, *9*, 5166−5178.
(62) Putro, P. A.; Liszulfah, R.; Isnaeni, I. The effect of poly(ethylene glycol) on the photoluminescence properties of carbon dots from cassava peels synthesized by hydrothermal methods. *SPEKTRA* **2019**, *4*, 11−20.
(63) Pan, Y.; Alam, M. A.; Wang, Z.; Huang, D.; Hu, K.; Chen, H.; Yuan, Z. One-step production of biodiesel from wet and unbroken microalgae biomass using deep eutectic solvent. *Bioresour. Technol.* **2017**, *238*, 157−163.
(64) Lu, W.; Alam, M. A.; Pan, Y.; Wu, J.; Wang, Z.; Yuan, Z. A new approach of microalgal biomass pretreatment using deep eutectic solvents for enhanced lipid recovery for biodiesel production. *Bioresour. Technol.* **2016**, *218*, 123−128.
(65) Ngatcha, A. D. P.; Muhammad, G.; Lv, Y.; Xiong, W.; Zhao, A.; Xu, J.; Alam, M. A. Microalgae biomass pre-treatment with deep eutectic solvent to optimize lipid isolation in biodiesel production. *Biomass Convers. Biorefin.* **2022**, *12* (1), 133−143.
(66) Muhammad, G.; Wang, J.; Xiong, W.; Lv, Y.; Zhang, S.; Zhao, A.; Jahanbakhsh-Bonab, P.; Solovchenko, A.; Xu, J.; Alam, M. A. Polyol based deep eutectic solvent-assisted pretreatment for enhanced lutein extraction from Chlorella pyrenoidosa. *J. Mol. Liq.* **2022**, *368*, No. 120775.

https://doi.org/10.1021/acsnanoscienceau.4c00048
ACS Nanosci. Au XXXX, XXX, XXX−XXX

(67) Kamdem, M. C. M.; Fouegue, A. D. T.; Lai, N. A comprehensive study on DES pretreatment application to microalgae for enhanced lipid recovery suitable for biodiesel production: combined experimental and theoretical investigations. *Energies* **2023**, *16*, No. 3806.
(68) Ozel, N.; Inam, A.; Elibol, M. Exploring deep eutectic solvents for enhanced extraction of bio-active compounds from microalgae biomass. *J. Mol. Liq.* **2024**, *407*, No. 125237.
(69) Wichaphian, A.; Sriket, N.; Sensupa, S.; Pekkoh, J.; Pathomaree, W.; Chromkaew, Y.; Suwannarach, N.; Kumla, J.; Cheirsilp, B.; Srinuanpan, S. Value-added green biorefinery co-products from ultrasonically assisted DES-pretreated Chlorella biomass. *Ultrason. Sonochem.* **2023**, *100*, No. 106628.
(70) de Almeida Pontes, P. V.; Shiwaku, I. A.; Maximo, G. J.; Batista, E. A. C. Choline chloride-based deep eutectic solvents as potential solvent for extraction of phenolic compounds from olive leaves: extraction optimization and solvent characterization. *Food Chem.* **2021**, *352*, No. 129346.
(71) Weber, S.; Grande, P. M.; Blank, L. M.; Klose, H. Insights into cell wall disintegration of Chlorella vulgaris. *PLoS One* **2022**, *17*, No. e0262500.
(72) Bao, L.; Liu, C.; Zhang, Z.-L.; Pang, D.-W. Photoluminescence-tunable carbon nanodots: surface-state energy-gap tuning. *Adv. Mater.* **2015**, *27*, 1663−1667.
(73) Duarte, T. A. G.; Pereira, R. F. P.; Medronho, B.; Maltseva, E. S.; Krivoshapkina, E. F.; Varela-Dopico, A.; Taboada, P.; Fu, L.; Ferreira, R. A. S.; de Zea Bermudez, V. A Glance at novel ionanofluids incorporating silk-derived carbon dots. *Chem. Mater.* **2024**, *36*, 1136−1152.
(74) Dias, L. M. S.; Fu, L.; Pereira, R. F. P.; Neto, A. N. C.; de Zea Bermudez, V.; André, P. S.; Ferreira, R. A. S. Evolving photonic authentication with sustainable luminescent smart e-tags. *FlexMat* **2024**, *1*, 116−126.
(75) Correia, S. F. H.; Fu, L.; Dias, L. M. S.; Pereira, R. F. P.; de Zea Bermudez, V.; André, P. S.; Ferreira, R. A. S. An autonomous power temperature sensor based on window-integrated transparent PV using sustainable luminescent carbon dots. *Nanoscale Adv.* **2023**, *5*, 3428−3438.
(76) Shiono, T.; Tando, F.; Nakano, H.; Sugahara, Y. Microstructural behavior of γ-Fe2O3 formation in reactions between layered iron oxychloride and sodium n-pentoxide. *Solid State Sci.* **2013**, *19*, 156−161.
(77) Concas, G. C.; Gisbert, M.; Cremona, M.; Lazaro, F.; da Costa, M. E. M. H.; De Barros, S. D. T.; Aucélio, R. Q.; Pierre, T. S.; Godoy, J. M.; Mendes, D.; Mariotto, G.; Daldosso, N.; Enrichi, F.; Cuin, A.; Ferreira, A. F.; de Azevedo, W. M.; Perez, G.; SantAnna, C.; Archanjo, B. S.; Fonseca, Y. E. L.; Rossi, A. L.; Deepak, F. L.; Khan, R.; Zaman, Q.; Reichenberger, S.; Fromme, T.; Margheri, G.; Sabino, J. R.; Fibbi, G.; Del Rosso, M.; Chillà, A.; Margheri, F.; Laurenzana, A.; Del Rosso, T. Pulsed-Laser-Driven CO2 Reduction Reaction for the Control of the Photoluminescence Quantum Yield of Organometallic Gold Nanocomposites. *Small Sci.* **2024**, *4*, No. 2300328.
(78) Rizzo, A. M.; Prussi, M.; Bettucci, L.; Libelli, I. M.; Chiaramonti, D. Characterization of microalga Chlorella as a fuel and its thermogravimetric behavior. *Appl. Energy* **2013**, *102*, 24−31.
(79) Binda, G.; Spanu, D.; Bettinetti, R.; Magagnin, L.; Pozzi, A.; Dossi, C. Comprehensive comparison of microalgae-derived biochar from different feedstocks: a prospective study for future environmental applications. *Algal Res.* **2020**, *52*, No. 102103.
(80) Presser, C.; Nazarian, A.; Ohaion-Raz, T.; Lerner, A.; Dubkin, H.; Dabush, B.; Danon, A.; Tal, O. P. Thermochemical behavior of Chlorella sp. and Chlamydomonas reinhardtii algae: Comparison of laser-driven calorimetry with thermogravimetric analysis. *Algal Res.* **2021**, *56*, No. 102325.
(81) Agrawal, A.; Chakraborty, S. A kinetic study of pyrolysis and combustion of microalgae Chlorella vulgaris using thermo-gravimetric analysis. *Bioresour. Technol.* **2013**, *128*, 72−80.
(82) Ghanem, A.; Al-Marjeh, R. A.-Q. B.; Atassi, Y. Novel nitrogen-doped carbon dots prepared under microwave-irradiation for highly sensitive detection of mercury ions. *Heliyon* **2020**, *6*, No. e03750.
(83) Taniguchi, M.; Bocian, D. F.; Holten, D.; Lindsey, J. S. Beyond green with synthetic chlorophylls − Connecting structural features with spectral properties. *J. Photochem. Photobiol., C* **2022**, *52*, No. 100513.
(84) Ding, H.; Yu, S.-B.; Wei, J.-S.; Xiong, H.-M. Full-color light-emitting carbon dots with a surface-state-controlled luminescence mechanism. *ACS Nano* **2016**, *10*, 484−491.
(85) Zhu, S.; Meng, Q.; Wang, L.; Zhang, J.; Song, Y.; Jin, H.; Zhang, K.; Sun, H.; Wang, H.; Yang, B. Highly photoluminescent carbon dots for multicolor patterning, sensors, and bioimaging. *Angew. Chem., Int. Ed.* **2013**, *52*, 3953−3957.
(86) Taniguchi, M.; Lindsey, J. S. Absorption and fluorescence spectral database of chlorophylls and analogues. *Photochem. Photobiol.* **2021**, *97*, 136−165.
(87) Grumbach, K. H.; Lichtenthaler, H. K.; Erismann, K. H. Incorporation of 14CO2 in photosynthetic pigments of Chlorella pyrenoidosa. *Planta* **1978**, *140*, 37−43.
(88) Simon, L.; Fodor, M.; Pais, I. Effects of zirconium on the growth and photosynthetic pigment composition of Chlorella pyrenoidosa green algae. *J. Plant Nutr.* **2001**, *24*, 159−174.
(89) Meng, X.; Chang, Q.; Xue, C.; Yang, J.; Hu, S. Full-colour carbon dots: from energy-efficient synthesis to concentration-dependent photoluminescence properties. *Chem. Commun.* **2017**, *53*, 3074−3077.
(90) Zhang, Y.; Xiao, J.; Zhuo, P.; Yin, H.; Fan, Y.; Liu, X.; Chen, Z. Carbon dots exhibiting concentration-dependent full-visible-spectrum emission for light-emitting diode applications. *ACS Appl. Mater. Interfaces* **2019**, *11*, 46054−46061.
(91) Wang, C.; Hu, T.; Wen, Z.; Zhou, J.; Wang, X.; Wu, Q.; Wang, C. Concentration-dependent color tunability of nitrogen-doped carbon dots and their application for iron(III) detection and multicolor bioimaging. *J. Colloid Interface Sci.* **2018**, *521*, 33−41.
(92) Tang, X.-D.; Yu, H.-M.; Nguyen, W.; Amador, E.; Cui, S.-P.; Ma, K.; Chen, M.-L.; Wang, S.-Y.; Hu, Z.-Z.; Chen, W. New Observations on Concentration-Regulated Carbon Dots. *Adv. Photonics Res.* **2023**, *4*, No. 2200314.
(93) Liu, J.; Yu, H.; Yang, S.; Feng, H.; Meng, H.; Wu, W.; Gao, Y. Concentration-dependent photoluminescence of carbon quantum dots useable in LED. *Langmuir* **2024**, *40*, 21524−21532.
(94) Hsiao, C.-J.; Lin, J.-F.; Wen, H.-Y.; Lin, Y.-M.; Yang, C.-H.; Huang, K.-S.; Shaw, J.-F. Enhancement of the stability of chlorophyll using chlorophyll-encapsulated polycaprolactone microparticles based on droplet microfluidics. *Food Chem.* **2020**, *306*, No. 125300.
(95) Wijesekara, T.; Xu, B. A critical review on the stability of natural food pigments and stabilization techniques. *Food Res. Int.* **2024**, *179*, No. 114011.
(96) Koca, N.; Karadeniz, F.; Burdurlu, H. S. Effect of pH on chlorophyll degradation and colour loss in blanched green peas. *Food Chem.* **2007**, *100*, 609−615.
(97) Wulandari, A.; Sunarti, T. C.; Fahma, F.; Enomae, T. The potential of bioactives as biosensors for detection of pH. *IOP Conf. Ser.: Earth Environ. Sci.* **2020**, *460*, No. 012034.
(98) Canjura, F. L.; Schwartz, S. J.; Nunes, R. V. Degradation kinetics of chlorophylls and chlorophyllides. *J. Food Sci.* **1991**, *56*, 1639−1643.
(99) Östbring, K.; Rayner, M.; Sjöholm, I.; Otterström, J.; Albertsson, P.-Å.; Emek, S. C.; Erlanson-Albertsson, C. The effect of heat treatment of thylakoids on their ability to inhibit in vitro lipase/co-lipase activity. *Food Funct.* **2014**, *5*, 2157−2165.
(100) Viera, I.; Herrera, M.; Roca, M. Influence of food composition on chlorophyll bioaccessibility. *Food Chem.* **2022**, *386*, No. 132805.
(101) Jin, M.; Jiang, S.; Wang, Y.; Wang, Y.; Guo, S.; Dong, X.; Qi, H. Formation of chlorophyll−anionic polysaccharide complex coacervates to improve chlorophyll color stability: thermodynamic and kinetic stability studies. *Int. J. Biol. Macromol.* **2024**, *275*, No. 133253.

https://doi.org/10.1021/acsnanoscienceau.4c00048
ACS Nanosci. Au XXXX, XXX, XXX−XXX

(102) Parray, Z. A.; Hassan, M. I.; Ahmad, F.; Islam, A. Amphiphilic nature of polyethylene glycols and their role in medical research. *Polym. Test.* **2020**, *82*, No. 106316.
(103) Laatsch, B. F.; Brandt, M.; Finke, B.; Fossum, C. J.; Wackett, M. J.; Lowater, H. R.; Narkiewicz-Jodko, A.; Le, C. N.; Yang, T.; Glogowski, E. M.; Bailey-Hartsel, S. C.; Bhattacharyya, S.; Hati, S. Polyethylene glycol 20k. Does it fluoresce? *ACS Omega* **2023**, *8*, 14208−14218.
(104) Chatterjee, D. P.; Pakhira, M.; Nandi, A. K. Fluorescence in "nonfluorescent" polymers. *ACS Omega* **2020**, *5*, 30747−30766.
(105) Bin, S.; Yu, J.; Tang, T.; Yuan, L.; Tang, Y. Study on UV Spectrum and Antioxidant Properties of 3-tert-Butyl-4-hydroxyanisole Molecule. *Russ. J. Phys. Chem. A* **2021**, *95*, 343−348.
(106) Hanke, E.; Schulz, U.; Kaatze, U. Molecular interactions in poly(ethylene glycol)−water mixtures at various temperatures: density and isentropic compressibility study. *ChemPhysChem* **2007**, *8*, 553−560.
(107) Trivedi, S.; Bhanot, C.; Pandey, S. Densities of {poly(ethylene glycol)+water} over the temperature range (283.15 to 363.15)K. *J. Chem. Thermodyn.* **2010**, *42*, 1367−1371.
(108) Muñoz, M. M.; Tinjacá, D. A.; Jouyban, A.; Martínez, F.; Acree, W. E. Volumetric properties of {PEG 200 (or 300) (1) + water (2)} mixtures at several temperatures and correlation with the Jouyban−Acree model. *Phys. Chem. Liq.* **2018**, *56*, 100−109.
(109) Hoga, H. E.; Torres, R. B.; Volpe, P. L. O. Thermodynamics properties of binary mixtures of aqueous solutions of glycols at several temperatures and atmospheric pressure. *J. Chem. Thermodyn.* **2018**, *122*, 38−64.
(110) Borodin, O.; Bedrov, D.; Smith, G. D. A molecular dynamics simulation study of polymer dynamics in aqueous poly(ethylene oxide) solutions. *Macromolecules* **2001**, *34*, 5687−5693.
(111) Hu, J.; Yamahara, H.; Liao, Z.; Yano, Y.; Tabata, H. Characterization of hydrogen bond network of waters around polyethylene glycol by broadband dielectric spectroscopy. *Appl. Phys. Lett.* **2022**, *120*, No. 023702.
(112) Boni, L. T.; Hui, S. W. The Mechanism of Polyethylene Glycol-Induced Fusion in Model Membranes. In *Cell Fusion*; Sowers, A. E., Ed.; Springer US: Boston, MA, 1987; pp 301−330.
(113) Lentz, B. R. PEG as a tool to gain insight into membrane fusion. *Eur. Biophys. J.* **2007**, *36*, 315−326.
(114) Rahman, M. M.; Hosano, N.; Hosano, H. Recovering microalgal bioresources: a review of cell disruption methods and extraction technologies. *Molecules* **2022**, *27*, No. 2786.
(115) André, P.; Ferreira, R.; Correia, S. F. H.; Georgieva, P.; Fu, L.; Antunes, M. A Comprehensive Dataset of Photonic Features on Spectral Converters in Energy Harvesting and Conversion Applications. *Sci. Data* **2024**, *11*, 50.

https://doi.org/10.1021/acsnanoscienceau.4c00048
ACS Nanosci. Au XXXX, XXX, XXX−XXX